Examining the requirement of TMED2 in murine placenta formation

Hannah Gordon

Department of Anatomy and Cell Biology

McGill University

Montreal, QC, Canada

July 2024

A thesis submitted to McGill University in partial fulfillment of the requirements of the degree of Master of Science

TABLE OF CONTENTS

Abstract

TMED2 is a cargo transporter expressed in the allantois and chorion and is required for placental labyrinth layer formation. Exchange between the maternal and fetal compartments occurs via the placental labyrinth layer. This is formed by attachment and fusion of the allantois and the chorion. The allantois and part of the chorion (chorionic mesothelium) are derived from extraembryonic mesoderm, and we postulate that TMED2 is required in the extraembryonic mesoderm for labyrinth layer formation. To examine the role of TMED2 in the extraembryonic mesoderm we used *Mesp1-Cre* and mutant mice with LoxP sequences flanking exons 2 and 3 of *Tmed2*. We first characterized this new exon 2-3 deletion by generating homozygous mutant (*Tmed2*$^{-/-}$) embryos which appear developmentally delayed and arrest by E8.5. Next, we collected *Tmed2*$^{loxp/loxp}$; *Mesp1*$^{Cre/+}$ embryos from Embryonic day (E) 9.5 – E12.5, for histological and morphological analysis. *Tmed2*$^{loxp/loxp}$; *Mesp1*$^{Cre/+}$ mutants have placental labyrinth layer formation, but arrest at E12.5. The labyrinth area was reduced in a subset of E9.5 and E10.5 mutants, and this difference was significant at E11.5. We used immunohistochemistry and *in situ* hybridization to examine the expression of proteins and genes essential for placenta formation and function. The number of cells expressing placental development genes is comparable in mutants and controls, while cells expressing the spongiotrophoblast marker, *Tpbpa*, were less abundant in mutants. Furthermore, various proteins including fibronectin, ITGA4, MCT1 and MCT4 appear to be mislocalized or not correctly transported. Our data indicates an essential role for TMED2 in the extraembryonic mesoderm for normal development of the placenta and labyrinth layer, which is potentially impaired due to disrupted intercellular communication from incorrect protein localization.

Résumé

TMED2 est un transporteur de cargo trouvé dans l'allantoïne et le chorion. TMED2 est nécessaire pour la formation du labyrinthe de placenta. La couche du labyrinthe est nécessaire pour l'échange entre les compartiments maternels et fœtaux. L'attachement et la fusion de l'allantoïne et du chorion forment le labyrinthe. L'allantoïne et une partie du chorion (le mésothélium chorionique) proviennent du mésoderme extraembryonnaire. Nous postulons que TMED2 est nécessaire dans le mésoderme extraembryonnaire pour la formation du labyrinthe de placenta. Pour examiner le rôle de TMED2 dans le mésoderme extraembryonnaire, nous avons utilisé des souris comportant *Mesp1-Cre* et les souris avec des séquences LoxP flanquant les exons 2 et 3 de *Tmed2*. Pour commencer, nous avons caractérisé cette nouvelle délétion de l'exon 2-3 de *Tmed2* en générant des embryons homozygotes mutants (*Tmed2*$^{-/-}$). Les *Tmed2*$^{-/-}$ embryons apparaissent retardés dans leur développement et s'arrêtent à E8,5, ce qui signifie que la délétion fonctionne. Ensuite, nous avons collecté des embryons *Tmed2*$^{loxp/loxp}$; *Mesp1*$^{Cre/+}$ de E9,5 - E12,5, pour examiner l'histologie et la morphologie. Les mutants *Tmed2*$^{loxp/loxp}$; *Mesp1*$^{Cre/+}$ ont la formation de la couche de labyrinthe placentaire, mais meurent à E12.5. La surface du labyrinthe est réduite dans les mutants à E9,5, E10,5 et E11,5. Nous avons utilisé l'immunohistochimie et l'hybridation *in situ* pour examiner l'expression des protéines et des gènes essentiels à la formation et à la fonction du placenta. Le nombre de cellules qui expriment des gènes importants pour le développement du placenta est comparable chez les mutants et les contrôles. Mais, le nombre de cellules qui expriment le marqueur du spongiotrophoblaste, *Tpbpa*, est réduit chez les mutants. Les protéines, fibronectine, ITGA4, MCT1 et MCT4, ne sont pas localisées ou transportées correctement. Nos données indiquent un rôle essentiel de TMED2 dans le mésoderme extraembryonnaire pour le développement normal du placenta et du labyrinthe.

Ceci est potentiellement altéré par la communication intercellulaire perturbée et la localisation incorrecte des protéines.

Acknowledgements

Firstly, I would like to begin by thanking my supervisor Dr. Loydie Jerome-Majewska for allowing me the opportunity to join her laboratory. I am very lucky to have had her mentorship, encouragement, help and guidance. Her support and the time in her lab have allowed me to grow as a person and professionally as a researcher. She has made my time in the lab a truly great experience that I have appreciated immensely.

I would like to thank my advisory committee, Dr. Chantal Autexier, Dr. David Hipfner, and Dr. Yojiro Yamanaka for their time, advice, and guidance on my thesis project.

Special thanks to all the past and present members of the Jerome-Majewska lab including Marie-Claude Beauchamp, Yanchen Dong, Shruti Kumar, Talia Marc, Casssandra Millet-Boureima, Joshua Moore, Sabrina Alam and Jennelle Smith. They have made this a very memorable and enjoyable time that I will always remember. I am thankful for all their teachings, support, shared knowledge, and the fun times.

I extend many thanks to my friends and family for their support and love. I would like to thank my dad, Mitchell, and my mom, Shirley, for always encouraging me and believing in me. I want to thank my sister, Elle, for being a great supporter and someone that I can always count on.

List of Figures

List of Tables

List of Abbreviations

BS-I	Bandeiraea simplicifolia-I
CD31	Cluster of differentiation 31
COP	Coat protein complex
COPI	Coat protein complex I
COPII	Coat protein complex II
DAPI	4′,6-diamidino-2-phenylindole
DE	Decidua
DNA	Deoxyribonucleic acid
E	Embryonic day
EC	Endothelial cell
EDTA	Ethylenediaminetetraacetic acid
ER	Endoplasmic reticulum
ERGIC	ER-Golgi intermediate complex
FV	Fetal vessel
GC	Giant cells
GCM1	Glial cell missing-1
GFP	Green fluorescent protein
GOLD	Golgi-dynamics domain
GPCR	G-protein coupled receptor
GPI	Glycosylphosphatidylinositol
H_2O_2	Hydrogen peroxide

ITGA4	Integrin alpha-4
LA	Labyrinth
MCT1	Monocarboxylate transporter 1
MCT4	Monocarboxylate transporter 4
mRNA	Messenger ribonucleic acid
MS	Maternal sinus
PBS	Phosphate-buffered saline
PFA	Paraformaldehyde
PL1	Placental lactogen-1
ST	Spongiotrophoblast
SynA	Syncytin-A
SynB	Syncytin-B
SynI	Syncytiotrophoblast-I
SynII	Syncytiotrophoblast-II
TMED	Transmembrane emp24 domain
TPBPA	Trophoblast specific protein alpha
VCAM1	Vascular cell adhesion molecule-1
mg	Milligram
mL	Milliliter
mm	Millimeter
µm	Micrometer

Contribution of Authors

Various authors have contributed to the results obtained in aim 1 and aim 2 of this project. Cassandra Millet-Boureima performed dissections of *Tmed2*$^{-/-}$ and *Tmed2*$^{loxp/loxp}$; *Mesp1*$^{Cre/+}$ mice in addition to Hannah Gordon. Talia Marc generated *Gcm1* and *Pl1* probes for *in situ* hybridization. Hannah Gordon performed all other experiments presented in this thesis. Dr. Loydie A. Jerome-Majewska designed and supervised this project.

CHAPTER I: INTRODUCTION AND LITERATURE REVIEW

1.1 Mouse placenta development

1.1.1 Placental layer development

The placenta is an organ essential for the continued development and growth of the embryo (Burton & Fowden, 2015; Panja & Paria, 2021). The mouse placenta is composed of layers of varying cell types, including the labyrinth layer, spongiotrophoblast layer, giant cell layer, and maternal decidua (Simmons et al., 2007). Two layers, the spongiotrophoblast layer and the giant cell layer, are known as the junctional zone of the placenta (Rusidzé et al., 2023; Watson & Cross, 2005). Mouse placenta development begins at embryonic day (E)3.5 with the formation of the blastocyst which contains two cell lineages: the inner cell mass and the trophectoderm (Simmons & Cross, 2005). Next on E4.5, successful implantation of the blastocyst must occur (Panja & Paria, 2021). The mural trophectoderm, not in contact with the inner cell mass, differentiates into polyploid trophoblast giant cells (John & Hemberger, 2012; Matsuo & Hiramatsu, 2017). Giant cells express placental lactogen-1 (*Pl1*) and have various functions, such as hormone secretion and aiding with implantation (Simmons et al., 2007). The polar trophectoderm, in contact with the inner cell mass, becomes the extraembryonic ectoderm and ectoplacental cone (Christodoulou et al., 2019; Gardner et al., 1973). Afterwards, the extraembryonic ectoderm differentiates into trophoblast chorion cells while the ectoplacental cone differentiates into spongiotrophoblast cells (Hu & Cross, 2011; Lawless et al., 2023; Watson & Cross, 2005). These spongiotrophoblast cells express the marker trophoblast specific protein alpha (*Tpbpa*) and will structurally support the placental labyrinth layer and play a role in

endocrine signaling (Hu & Cross, 2011; John & Hemberger, 2012). The development of these cellular layers in the junctional zone of the placenta occurs by E9.5 (Elmore et al., 2022).

The allantois and chorion are two key tissues that generate the labyrinth layer of the placenta (Hou et al., 2016; Rinkenberger & Werb, 2000). To form these tissues, the inner cell mass of the blastocyst differentiates into the extraembryonic primitive endoderm (hypoblast) and the epiblast (Morris, 2011). From the epiblast, the allantois will develop; the allantois is derived from extraembryonic mesoderm and will bud from the primitive streak (Downs, 2022; Watson & Cross, 2005). Whereas the chorion is partially extraembryonic ectoderm-derived and partially extraembryonic mesoderm-derived (Panja & Paria, 2021).

1.1.2 Chorioallatnoic attachment and fusion

The chorion and allantois must undergo attachment and fusion for complete labyrinth layer development (Stecca et al., 2002). Chorioallantoic attachment (Figure 1.1) between the vascular allantois and the chorion occurs at E8.5 (Watson & Cross, 2005). Attachment involves the ligand vascular cell adhesion molecule-1 (VCAM1), on the allantois surface, which will bind to its receptor integrin alpha-4 (ITGA4) on the chorion mesothelium, an extraembryonic mesoderm-derived tissue (Cross et al., 2003; Gurtner et al., 1995). This binding of VCAM1 and ITGA4 aids in the alignment and contact of the chorion and allantois (Inman & Downs, 2007; Kwee et al., 1995). Afterwards, fusion and branching occurs where the chorion folds to make villi for fetal blood vessel growth from the allantois (Watson & Cross, 2005). Branching requires a process called branch-point selection where the location of initial branching is determined by the expression of an essential transcription factor, Glial cell missing-1 (*Gcm1*) (Cross et al., 2003). *Gcm1* expression increases at E8.5 in clusters of chorionic trophoblast cells for selection

and *Gcm1* will be expressed in the tips of the branches (Anson-Cartwright et al., 2000; Basyuk et al., 1999). Branching allows for the increase of surface area in the placenta for efficient nutrient and gas exchange (Cross et al., 2006; Woods et al., 2018).

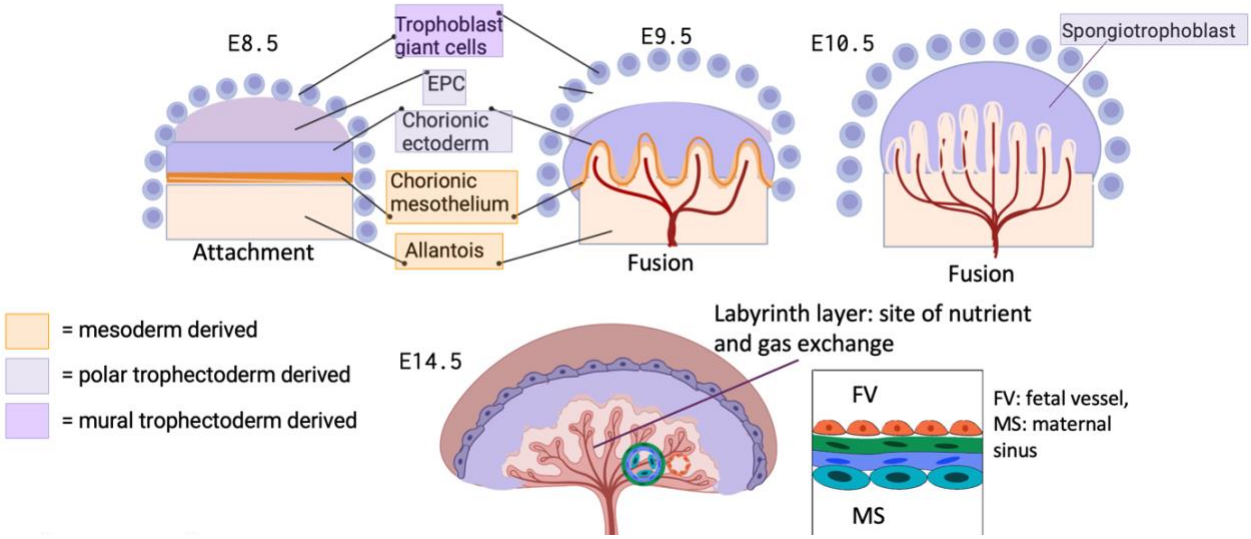

Figure 1.1 Chorioallantoic attachment and fusion of the murine placenta. Attachment between the chorion and allantois surfaces occurs at E8.5. Depiction of fusion and branching between the cell layers occuring after attachment to create the labyrinth layer of the placenta. The labyrinth layer includes vasculature of maternal sinuses (MS) and fetal vessels (FV). The allantois and a portion of the chorion, the chorionic mesothelium (orange) are extraembryonic mesoderm-derived. Created in BioRender.

The labyrinth layer of the placenta is the site of exchange between the embryo and the mother through fetal vessels and maternal sinuses (Nadeau & Charron, 2014). The syncytiotrophoblast bilayer separates the fetal vessels and sinusoidal maternal blood sinuses

(Jiang et al., 2023; Watson & Cross, 2005). To form the syncytiotrophoblast cells in the labyrinth, chorionic trophoblast cells differentiate into a syncytiotrophoblast bilayer through cell fusion (Jiang et al., 2023). In addition, *Gcm1* expression is needed for the differentiation of the syncytiotrophoblast cells (Anson-Cartwright et al., 2000). The syncytiotrophoblast bilayer includes syncytiotrophoblast-I and syncytiotrophoblast-II cell layers that are connected by tight junctions (Lawless et al., 2023; Shaha et al., 2023). These layers are involved in maintaining exchange between the embryo and the mother and separating their contents (John & Hemberger, 2012). Additionally, the maternal sinuses and fetal vessels of the placenta allow for the exchange of nutrients and gases through the countercurrent flow of blood in these vessels (Adamson et al., 2002). Fetal vessels are lined by endothelial cells derived from the allantois and sinusoidal trophoblast giant cells line the maternal blood sinuses (Tai-Nagara et al., 2017). The development of the placental vasculature in the labyrinth creates the functional hemochorial mouse placenta (Soares et al., 2018).

1.2 Secretory pathway

The secretory pathway is needed for the synthesis and transport of transmembrane and secreted proteins (Figure 1.2) (Aber et al., 2019; Pelham, 1996). Protein synthesis of secretory proteins and transmembrane proteins begins at the ER (endoplasmic reticulum) and starts the process of anterograde protein transport to the correct cellular destination (Barlowe & Miller, 2013). The ER has several functions including protein quality control, translocation, post-translation modifications and protein folding (Schwarz & Blower, 2016). Proteins will then exit the ER through ER exit sites and are sorted into COPII-coated vesicles (Duden, 2003). The vesicles will be transported to the ER-Golgi intermediate complex (ERGIC) which acts as a

transport complex while ensuring quality control of new proteins (Appenzeller-Herzog, 2006). These proteins will enter the Golgi for continued protein processing and sorting (Donaldson & Lippincott-Schwartz, 2000). Next, proteins will be transported to the cell surface membrane, secretory vesicles or endosomes and lysosomes (Luzio et al., 2014). Proteins can also be trafficked in the retrograde direction from the Golgi back to the ER through COPI-coated vesicles to recycle machinery or return misfolded proteins (Cole et al., 1998; Spang, 2013).

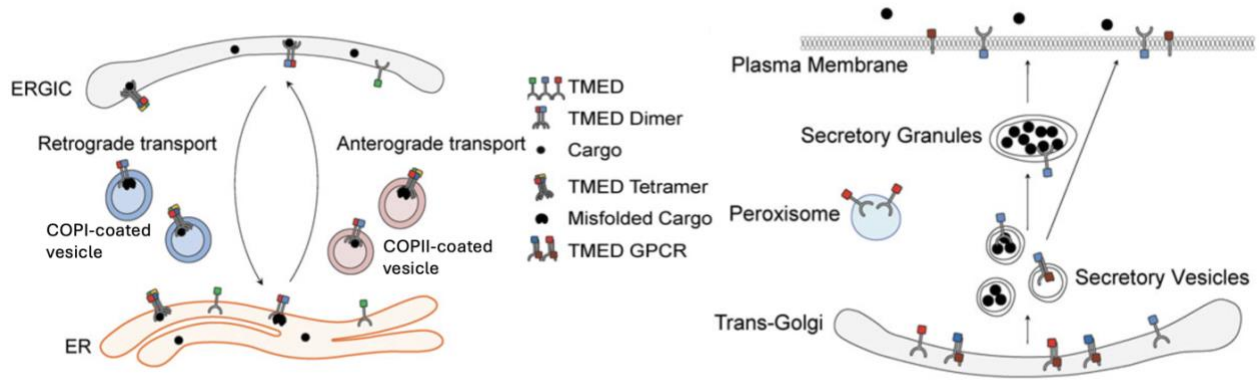

Figure 1.2 TMED proteins are located in the secretory pathway for cargo transport. The secretory pathway includes protein synthesis in the ER and transport in the anterograde direction using COPII-coated vesicles for transport to the Golgi. Retrograde transport uses COPI-coated vesicles for transport back to the ER. TMED proteins within COP-coated vesicles are used for cargo protein transport. Furthermore, TMED proteins are found in the ER, Golgi, plasma membrane, secretory granules, and vesicles (Adapted from Aber et al., 2019).

1.3 TMED proteins

The transmembrane emp24 domain (TMED) family is a group of proteins that transport various cargo proteins between the endoplasmic reticulum and the Golgi in the secretory pathway (Aber et al., 2019; Dominguez et al., 1998). TMED proteins will bind to COP-coated vesicles to act as cargo receptors and bring cargo in both the anterograde and retrograde direction (Figure 1.2) (Strating & Martens, 2009). TMED proteins are classified as type I transmembrane proteins and consist of several functional domains (Carney & Bowen, 2004). The Golgi-dynamics domain (GOLD) assists TMED dimerization through protein interactions and bonds, the cytoplasmic tail binds COP proteins, the signal sequence allows for ER translocation, the coiled-coil domain is involved in oligomerization and the transmembrane domain binds lipids, sorts proteins and forms vesicles (Nagae et al., 2016; Roberts & Satpute-Krishnan, 2023). There are ten mammalian *Tmed* genes divided into four subfamilies: α (*Tmed4, Tmed9, Tmed11*), β (*Tmed2*), γ (*Tmed1, Tmed3, Tmed5, Tmed6, Tmed7*) and δ (*Tmed10*) (Zhou et al., 2023). Previously known TMED cargos include glycosylphosphatidylinositol (GPI)-anchored proteins, Wnt ligands and G-protein coupled receptors (GPCRs) (Buechling et al., 2011; Luo et al., 2007; Marzioch et al., 1999).

1.4 TMED2

1.4.1 Tmed2 expression

Tmed2 gene expression in mice has been documented in the placenta and embryo (Jerome-Majewska et al., 2010). In mice, at E5.5, *Tmed2* is expressed in both the embryonic and extraembryonic tissues (Jerome-Majewska et al., 2010). At E6.5, *Tmed2* levels are increased in

the ectoplacental cone and extraembryonic ectoderm (Jerome-Majewska et al., 2010). By E8.5, *Tmed2* expression is found within the heart and was shown to be expressed at later developmental stages throughout the embryo (Jerome-Majewska et al., 2010). In the murine placenta at E8.5, *Tmed2* is expressed in the chorion, allantois, and giant cells (Jerome-Majewska et al., 2010). At E9.5 and E10.5, *Tmed2* is localized in the giant cells, spongiotrophoblasts and labyrinth layer of the placenta (Jerome-Majewska et al., 2010). Thus, indicating expression of *Tmed2* is present throughout the embryonic and placental tissues during development.

1.4.2 TMED2 cargo proteins

A key function of TMED2 is its ability to act as a cargo transporter; several cargo proteins of TMED2 have been identified in previous studies. TMED2 and its orthologues have been examined in several models including cell culture, yeast, *C. elegans* and mice. One potential TMED2 cargo is fibronectin, an extracellular matrix protein, as it is retained within the ER of murine placental cells in the absence of TMED2 (Hou & Jerome-Majewska, 2018; Singh et al., 2010). Another potential cargo is VCAM1, a cell adhesion molecule, which is abnormally localized in the murine placenta in the absence of TMED2 (Hou & Jerome-Majewska, 2018).

In yeast, Gas1p, a GPI-anchored protein, is incorrectly transported when p24, a TMED2 orthologue, is mutated (Marzioch et al., 1999; Stirling et al., 1992). Additionally, invertase, an enzyme for sucrose hydrolysis, is not transported properly when the p24 complex is mutated (Muniz et al., 2000). Furthermore, in yeast without functional p24, there is increased extracellular secretion of Kar2p/BiP, a yeast ER chaperone (Belden & Barlowe, 2001; Okamura et al., 2000). Another study used *C. elegans* as a model with mutations in the TMED2 orthologue *sel-9* and identified increased transport of mutated LIN-12 and GLP-1 receptors (Wen &

Greenwald, 1999). Also, Minin et al. mutated TMED2 in embryonic stem cells and found increased Smoothened protein, a GPCR in the hedgehog pathway, at the plasma membrane (Minin et al., 2022). Thus, TMED2 can act as a cargo transporter of a variety of proteins, and some of these studies above using mutant TMED2 models reveal the role of TMED2 in the negative regulation of protein transport (Belden & Barlowe, 2001; Minin et al., 2022; Okamura et al., 2000; Wen & Greenwald, 1999).

1.4.3 TMED2 99J mutation

The 99J point mutation is a missense mutation that was identified in the TMED2 signal sequence (Jerome-Majewska et al., 2010). Homozygous 99J mutant embryos contain mRNA levels equal to wildtype controls while embryonic protein levels are decreased, likely due to impaired translocation into the ER (Jerome-Majewska et al., 2010). These mutant embryos are developmentally delayed and die by E11.5 (Jerome-Majewska et al., 2010). Placenta histology displays the absence of the labyrinth layer (Figure 1.3), the cause of embryonic lethality, as well as no spongiotrophoblast layer along with no allantois invagination (Jerome-Majewska et al., 2010). *In situ* hybridization of the homozygous *Tmed2*$^{99J/99J}$ mutants showed both *Tpbpa* and *Gcm1* had an abnormal or reduced expression pattern (Jerome-Majewska et al., 2010).

Furthermore, Hou & Jerome-Majewska used an explant model to examine the *Tmed2*$^{99J/99J}$ mutation with transgenic mouse lines expressing eGFP+ cells or tdTomato cells to examine chorioallantoic attachment (Hou & Jerome-Majewska, 2018). When both the chorion and allantois contained the 99J mutation or when only the chorion was mutated, 50% of the sample failed to attach while the other 50% underwent chorioallantoic attachment but failed to fuse (Hou & Jerome-Majewska, 2018). When just the mesoderm-derived allantois is mutated,

attachment occurs, but fusion is limited to a smaller region (Hou & Jerome-Majewska, 2018). These results indicate the requirement of TMED2 in both the chorion and allantois for complete labyrinth layer formation and normal placental development.

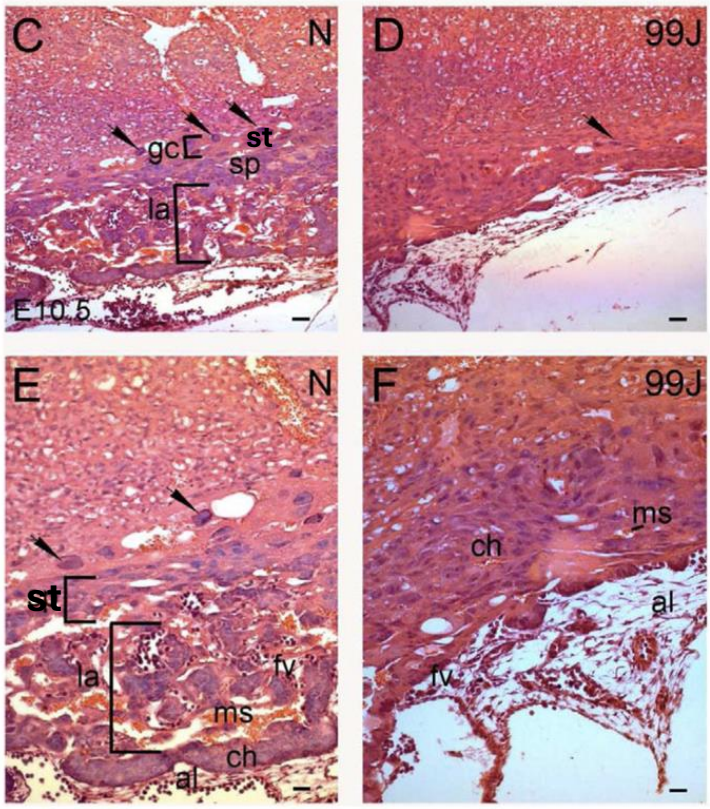

Figure 1.3 The labyrinth layer is absent in E10.5 *Tmed2*$^{99J/99J}$ mutant placentas. Control (C, E) E10.5 placenta with the presence of normal placenta landmarks including the labyrinth layer (la), giant cells (gc), spongiotrophoblasts (st), maternal sinuses (ms), fetal vessels (fv), chorion (ch), and allantois (al). In *Tmed2*$^{99J/99J}$ mutant (D, F) placentas, there is an absence of the labyrinth layer and spongiotrophoblast layer. Scale bars: 50-µm (C, D) and 20-µm (E, F) (Adapted from Jerome-Majewska et al., 2010)

1.5 Hypothesis and Aims

1.5.1 Hypothesis

The previous work from the Jerome-Majewska lab using the 99J mutation showed that TMED2 was needed in both the chorion, a partially ectoderm and mesoderm-derived tissue, and the allantois, a mesoderm-derived tissue for labyrinth layer development (Hou & Jerome-Majewska, 2018). Based on these studies, we hypothesized that TMED2 is required in the extraembryonic mesoderm for placental labyrinth layer formation.

1.5.2 Aims

To examine the hypothesis, the following aims were established:

1. Investigate a new *Tmed2* exon 2-3 deletion allele in *Tmed2*$^{-/-}$ embryos and compare whether this deletion produces similar outcomes to the *Tmed2*$^{99J/99J}$ mutation.
2. Remove TMED2 from the extraembryonic mesoderm, with the exon 2-3 deletion, and assess whether TMED2 is required in these structures for chorioallantoic attachment and fusion.

CHAPTER II: MATERIALS AND METHODS

2.1 Animals

Mice work was done according to the Canadian Council on Animal Care and approved by the Animal Care Committee of the Research Institute of the McGill University Health Center. *Tmed2*$^{+/-}$ and *Tmed2*$^{loxp/+}$ mice were maintained on a mixed CD1 and C57BL/6 genetic background. Mice carrying *Mesp1-Cre* used in experiments were from a mixed CD1 and C57BL/6 genetic background.

2.1.1 Tmed2$^{-/-}$ *mutants.*

To examine the homozygous deletion of *Tmed2,* I used a conditional mutant *Tmed2* line with LoxP sequences flanking exons 2 and 3 of the allele. Previously, *ß-actin-Cre* was used to generate heterozygous *Tmed2* mice (*Tmed2*$^{+/-}$) carrying the exon 2-3 deletion which were then set up together to obtain homozygous *Tmed2*$^{-/-}$ embryos.

2.1.2 Tmed2$^{loxp/loxp}$*; Mesp1*$^{Cre/+}$ *mutants*

To generate *Tmed2*$^{loxp/loxp}$; *Mesp1*$^{Cre/+}$ mutants, I used the conditional mutant *Tmed2* line with LoxP sequences flanking exons 2 and 3. Then, I used *Tmed2*$^{loxp/+}$ mice carrying *Mesp1-Cre* (*Mesp1*$^{Cre/+}$) set up with *Tmed2*$^{loxp/+}$ mice to obtain conditional homozygous (*Tmed2*$^{loxp/loxp}$; *Mesp1*$^{Cre/+}$) mutant embryos and placentas with two *Tmed2* deletion alleles in the mesoderm-derived cells. Placentas were collected between E9.5-E12.5.

2.2 Genotyping

DNA was extracted from mouse ear punches or yolk sacs with alkaline lysis (25 mM NaOH, 0.2 mM EDTA) at 95℃ for 30 minutes then neutralized with neutralization buffer (40 mM Tris-HCl pH 5.0). Genotyping was used to identify the *Tmed2* WT allele (199 bp), LoxP allele (233 bp) or presence of the deletion allele (261 bp). *Tmed2* was genotyped using a three-primer PCR with the following primers:

Tmed2 F1: 5'-ACATTTCGCTTGGACAGGTAA-3'

Tmed2 F3: 5'-AGTGGTAGCTCTCCCTTAGCA-3'

Tmed2 R3: 5'-AGGGGAGAACCAATTCAGCAT-3'.

The program for *Tmed2* genotyping used is as follows: 95°C 3 min, 95°C 30 sec, 52°C 30 sec, 72°C 30 sec for 40 cycles then 72°C 5 min.

Mesp1-Cre was genotyped with the following primers to identify mutant (400 bp) and internal control (200 bp) alleles:

Mesp1-Cre F: 5'-TGCCACGACCAAGTGACAGCAATG-3'

Mesp1-Cre R: 5'-ACCAGAGACGGAAATCCATCGCTC-3'

Internal Control F: 5'-CAAATGTTGCTTGTCTGGTG-3'

Internal Control R: 5'-GTCAGTCGAGTGCACAGTTT-3'

mT/mG was genotyped with the following primers to identify mutant (128 bp) and WT (212 bp) alleles:

mT/mG F: 5'-TAGAGCTTGCGGAACCCTTC-3'

WT F: 5'-AGGGAGCTGCAGTGGAGTAG-3'

Common R: 5'-CTTTAAGCCTGCCCAGAAGA-3'

The program used for *Mesp1-Cre* and mT/mG is as follows: 94°C 2 min, 95°C 20 sec, 65°C 15 min (-0.5°C per cycle), 68°C 10 sec for 10 cycles. Next, 94°C 15 sec, 62°C 15 sec, 72°C 10 sec for 28 cycles then 72°C 2 min.

2.3 Embryo and placenta collection

To collect embryos and placentas, the day of plug was considered embryonic day 0.5 (E0.5). Yolk sacs were used for genotyping of placentas and embryos. Embryos and placentas were dissected in phosphate-buffered saline (PBS) and fixed in 4% PFA at 4°C overnight unless otherwise noted. Placentas were then cut at the midway point and dehydrated in ethanol washes for paraffin embedding. The tissue was sectioned at 7μm thickness and stained with Hematoxylin and Eosin.

2.4 Immunofluorescence

Immunofluorescence was performed on paraffin embedded sections according to standard protocols (Zakariyah et al., 2012). The primary antibodies used include: MCT1 (1:100 dilution, Sigma, ab1286-I), MCT4 (1:100 dilution, Millipore, ab3314p), Fibronectin (1:100 dilution, Abcam, ab23750), CD31 (1:100 dilution, Abcam, ab28364), KDEL (1:100 dilution conjugated, Abcam, ab203421), VCAM1 (1:100 dilution, Santa Cruz, SC-1504), ITGA4 (1:100 dilution, Abcam, ab25247). The secondary antibodies used include Alexa Fluor 488 and 568 (1:500 dilution, Invitrogen). Antigen retrieval for GFP (1:250 dilution conjugated, Invitrogen, A21311) was done with Tris-EDTA (pH 9.0). Images were taken on Leica microsystem

(DMI6000B) and Leica camera (model DFC450). Confocal images were taken on a Zeiss LSM880 laser scanning confocal microscope.

2.5 *In situ* hybridization

Pl1, Gcm1, Tpbpa, Syncytin-A and *Syncytin-B* riboprobes were used and *in situ* hybridization was performed on paraffin sections as previously described (Simmons et al., 2008). To generate antisense probes, the Qiagen plasmid midi prep kit protocol was followed. Plasmids (20 µg) were linearized with the appropriate restriction enzyme (5 µl) and buffer (10 µl) in a 100 µl reaction with ddH_2O at 37°C for 2 hours minimum (*Pl1*: HindIII CutSmart buffer*, Gcm1*: XhoI CutSmart buffer*, Tpbpa*: EcoRI EcoRI buffer, *Syncytin-A*: SpeI CutSmart buffer, *Syncytin-B*: SpeI CutSmart buffer). Purification was done using the QIAquick PCR purification kit following the listed protocol. Pure linear plasmid (1 µg) was combined with DIG mix (2 µl), transcription buffer (2 µl) and the appropriate RNA polymerase (2 µl) in a 20 µl reaction with DEPC H_2O at 37°C for 2 hours (Sp6: *Pl1, Tpbpa, Syncytin-A,* T7: *Gcm1*, *Syncytin-B*). Samples were then treated with DNAse I for 15 min at 37°C before stopping the reaction with 0.2M EDTA. Samples were then precipitated and the pellet was dissolved in 50 µl of DEPC H_2O. Successful reactions were confirmed by running a gel with the probes and performing a dot blot. Final probe concentration used for *in situ* hybridization is 0.05 µg/ml.

2.6 Placenta area

Placenta area was measured using ImageJ with H&E-stained placenta sections. This was done on sections at the midway point of the placenta where the chorionic plate is visible.

Measurements were repeated three times per placenta sample at approximately 28-µm between measurements.

2.7 Immunohistochemistry

Immunohistochemistry was performed on paraffin embedded sections using an antibody for Lectin from *Bandeiraea simplicifolia* (BS-I) (1:100 dilution, L2895, Sigma). Slides were deparaffinized with xylene and rehydrated with graded ethanol washes then rinsed with PBS. Antigen retrieval was done using 10mM sodium citrate buffer (pH 6.0) before rinsing with PBS. Slides were treated with 3% H_2O_2 for 15 minutes then blocked with 10% horse serum in PBS/0.3% Triton-X100 in a humid chamber for 1 hour. Slides were incubated overnight at 4°C in a humid chamber with antibody diluted in 10% horse serum in PBS/0.3% Triton-X100. One drop of DAB substrate was diluted in 1ml of buffer and applied to slides to develop colour. Slides were rinsed in water then counterstained with hematoxylin for 45 sec. Slides were rinsed again in water before dehydrating with ethanol washes and mounting.

2.8 Statistical Analysis

Microsoft Excel and GraphPad Prism were used for statistical analyses. To determine Mendelian segregation and genotype distribution, Chi-Squared test was used. One-way ANOVA was used to analyze embryo and placenta weight. Two sample t-Test was used for placental area measurement analyses. P-values < 0.05 were considered significant.

CHAPTER III: RESULTS

Aim 1

3.1 *Tmed2*$^{-/-}$ embryos begin to resorb and arrest by E8.5

We first examined the homozygous exon 2-3 deletion of *Tmed2* using heterozygous mice containing one *Tmed2* deletion allele (Fig. 3.1 A). Next, these heterozygous (*Tmed2*$^{+/-}$) mice were mated together to collect *Tmed2*$^{+/+}$, *Tmed2*$^{+/-}$, and *Tmed2*$^{-/-}$ mutant embryos between E6.5-E10.5 (Fig. 3.1 A, Table 3.1). At E9.5 and E10.5, there are no homozygous mutant (*Tmed2*$^{-/-}$) embryos that survive to this point and those that we were able to genotype were resorbed (Table 3.2). At E8.5, we found that some of the *Tmed2*$^{-/-}$ embryos (n=7/35) were resorbing and the majority of E8.5 *Tmed2*$^{-/-}$ embryos were arrested by this point. Thus, we were able to conclude that the homozygous exon 2-3 deletion of *Tmed2* leads to arrest by E8.5 and this mutation is more severe than the previous 99J mutation. Genotypic distribution between E6.5 to E10.5 is consistent with the expected Mendelian segregation.

Table 3.1. Genotype distribution table of *Tmed2*$^{-/-}$ embryos by embryonic stage.

Stage	*Tmed2*$^{+/+}$ (resorbed)	*Tmed2*$^{+/-}$ (resorbed)	*Tmed2*$^{-/-}$ (resorbed)
E6.5	1	4	2
E7.5	1	11	2
E8.5	47 (3)	104 (5)	35 (7)
E9.5	8 (2)	13 (2)	2 (2)
E10.5	6 (1)	23 (5)	6 (6)

3.2 E8.5 *Tmed2*$^{-/-}$ embryos are developmentally delayed and resemble E7.5 control embryos

We conducted dissections and examined embryos to phenotypically compare these *Tmed2*$^{-/-}$ mutants to the *Tmed2*$^{99J/99J}$ missense mutation. We focused on E8.5 embryos since this is the point where these mutants arrest. Wildtype (*Tmed2*$^{+/+}$) embryos at E8.5 are alive and contain defining features and structures including the heart and somites (Fig. 3.1 B). At E8.5, heterozygous embryos (*Tmed2*$^{+/-}$) containing one wildtype allele and one deletion allele have a similar morphological appearance to wildtype embryos and generally appear normal (Fig. 3.1 C). Heart and somites are both present in the heterozygous embryos (*Tmed2*$^{+/-}$). However, homozygous mutant embryos (*Tmed2*$^{-/-}$) containing the exon 2-3 deletion of *Tmed2* appear developmentally delayed (Fig. 3.1 D). The *Tmed2*$^{-/-}$ embryos do not have heart or somites. Only the embryonic and extraembryonic regions are clearly defined in the *Tmed2*$^{-/-}$ mutant embryos (Fig. 3.1 D). Therefore, we can conclude that one wildtype allele of *Tmed2* is sufficient to maintain normal embryonic development. Additionally, the homozygous exon 2-3 deletion of *Tmed2* (*Tmed2*$^{-/-}$) produces a developmentally delayed embryo that appears similar to normal E7.5 embryos (Fig. 3.2A).

To continue to characterize the consequences of the *Tmed2*$^{-/-}$ mutation, we did earlier dissections at E7.5. We did not identify any resorptions of the *Tmed2*$^{-/-}$ mutant embryos at E7.5. At this stage, *Tmed2*$^{+/+}$ and *Tmed2*$^{+/-}$ embryos are similar in size and appearance with distinguishable embryonic and extraembryonic regions (Fig. 3.2A, B). In comparison, the *Tmed2*$^{-/-}$ mutant embryos are slightly smaller and appear marginally delayed at this stage (Fig. 3.2C). This provides further evidence that at early developmental stages, this exon 2-3 deletion of *Tmed2* (*Tmed2*$^{-/-}$) begins to prevent normal embryonic and extraembryonic development.

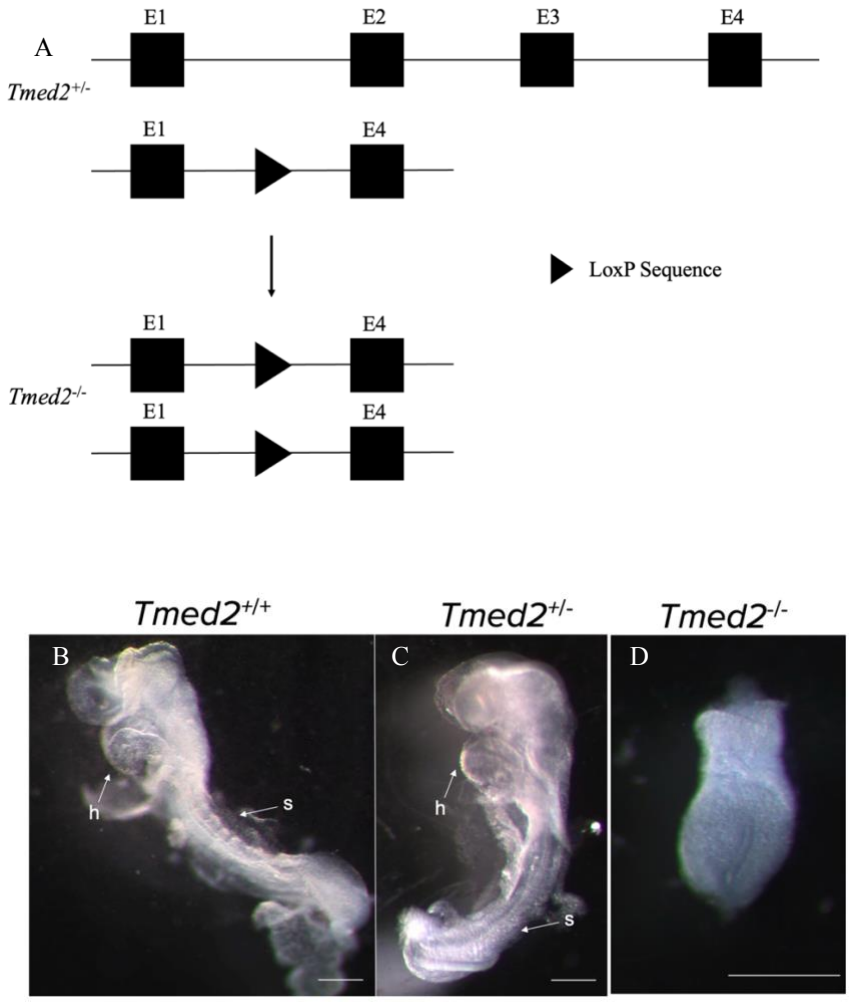

Figure 3.1. Homozygous exon 2-3 deletion of TMED2 causes developmental delay. (A) *Tmed2* heterozygous (*Tmed2*$^{+/-}$) allele representation with one wildtype allele of *Tmed2* containing four exons and the deletion allele without exons 2 and 3. Homozygous mutant (*Tmed2*$^{-/-}$) allele representation with two deletion alleles. (B) Representative image of wildtype control embryo (*Tmed2*$^{+/+}$) at E8.5 contains visible heart (h) and somites (s). (C) Representative image of heterozygous embryo (*Tmed2*$^{+/-}$) at E8.5 contains visible heart and somites. (D) Representative image of homozygous mutant embryo (*Tmed2*$^{-/-}$) at E8.5 is developmentally

delayed and lacks characteristic features of the control embryo. Scale bar: 250-µm (B, C) and 500-µm (D)

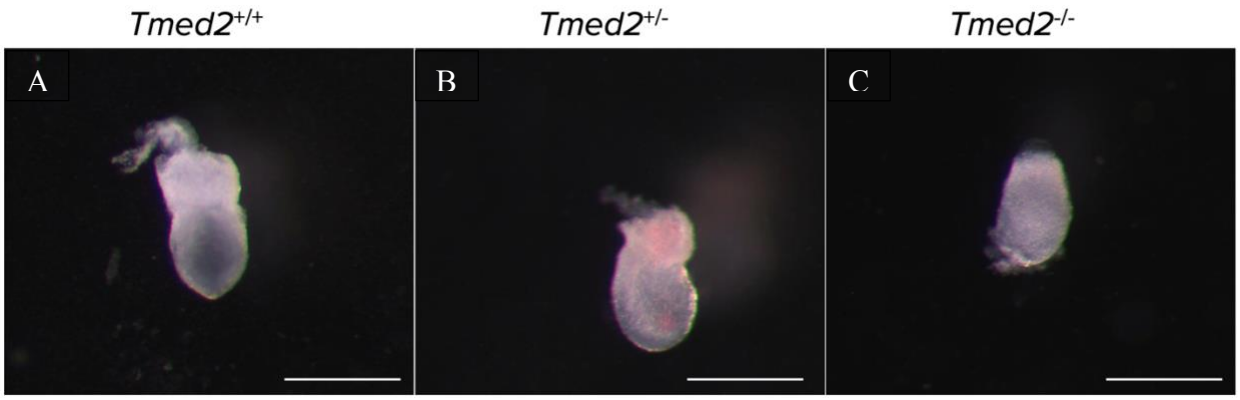

Figure 3.2. E7.5 *Tmed2*$^{-/-}$ embryos are smaller than *Tmed2*$^{+/+}$ controls. (A) Representative image of wildtype control embryo (*Tmed2*$^{+/+}$) with distinct embryonic and extraembryonic regions. (B) Representative image of a heterozygous embryo (*Tmed2*$^{+/-}$) is similar to the control with clear embryonic and extraembryonic regions. (C) Representative image of homozygous mutant embryo (*Tmed2*$^{-/-}$) at E7.5 is similar to the control but smaller and less developed. Scale bar: 500-µm

Aim 2

In aim 1, we were able to identify that the new homozygous *Tmed2* exon 2-3 deletion leads to developmental delay and embryonic arrest by E8.5. Thus, we used the same exon 2-3 deletion of *Tmed2* in aim 2 to conditionally remove TMED2 from the extraembryonic mesoderm using *Mesp1-Cre.* This allows us to address our question: what happens to placental labyrinth layer development when TMED2 is absent from the extraembryonic mesoderm? We hypothesize that this deletion in the extraembryonic mesoderm will prevent labyrinth layer development and proper placenta formation.

3.3 *Mesp1-Cre* is active in the mouse placenta of both controls and *Tmed2*$^{loxp/loxp}$; *Mesp1*$^{Cre/+}$ mutants

To remove TMED2 from the extraembryonic mesoderm, I used Cre-LoxP recombination where Cre recombinase will recognize two LoxP sites and remove the DNA in between (Kim et al., 2018). This system allows one to develop a conditional deletion model depending on which promoter is controlling Cre (Kim et al., 2018). I used a mutant mouse line containing LoxP sequences flanking exons 2 and 3 of the *Tmed2* gene along with Cre that has been knocked in the *Mesp1* locus for conditional deletion (Fig. 3.3A) (Liu et al., 2016). *Mesp1* expression begins at E6.5 in the mesodermal cells at the primitive streak (Saga et al., 1996). When *Tmed2* contains the LoxP sites (*Tmed2*$^{loxp/loxp}$) and is in the presence of *Mesp1-Cre* (*Mesp1*$^{Cre/+}$), this produces two deletion alleles of *Tmed2* in all the mesoderm-derived cells that have expressed *Mesp1* (Yang et al., 2020). We use the heterozygous knock-in *Mesp1*$^{Cre/+}$ since *Mesp1*$^{Cre/Cre}$ mice die by E10.5 and their mesoderm cell migration is disrupted (Saga et al., 1999). Previous lineage tracing of *Mesp1*$^{-}$*Cre* using ROSA-LacZ has shown expression in the placenta allantois, fetal endothelial

cells, heart, and amnion (Saga et al., 1999; Yang et al., 2020). To confirm the location of the mesoderm-derived cells in our mutant placentas, we introduced the ROSA mT/mG reporter into the mutant *Tmed2* mouse line and mated them with mice containing *Mesp1-Cre.* This reporter produces tdTomato fluorescence in all cells but in the presence of Cre, tdTomato is excised and EGFP fluorescence will be produced (Muzumdar et al., 2007). Therefore, the *Mesp1*-derived cells will fluoresce green and express GFP. I used sections of E11.5 control (n=2) and *Tmed2*$^{loxp/loxp}$; *Mesp1*$^{Cre/+}$ mutant (n=3) placentas with an antibody for GFP. In the *Tmed2*$^{+/+}$; *Mesp1*$^{Cre/+}$ controls, the majority of GFP+ cells are within the placental labyrinth layer along with a few cells that appear within the junctional zone of the placenta (white arrow) (Fig. 3.3 B1-B4). Similarly, in *Tmed2*$^{loxp/loxp}$; *Mesp1*$^{Cre/+}$ mutant placentas the GFP+ cells are mainly concentrated in the labyrinth layer with some cells that appear in the junctional region of the placenta (white arrow) (Fig. 3.3 C1-C4). This indicates *Mesp1-Cre* activity is present in both mutant and control placenta. These mesoderm-derived cells contribute mainly to the labyrinth layer of the placenta and may influence the neighbouring cells in the junctional zone

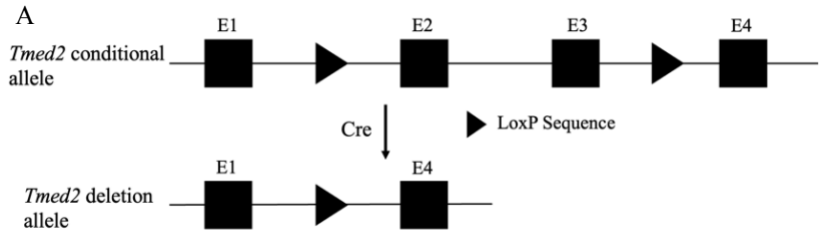

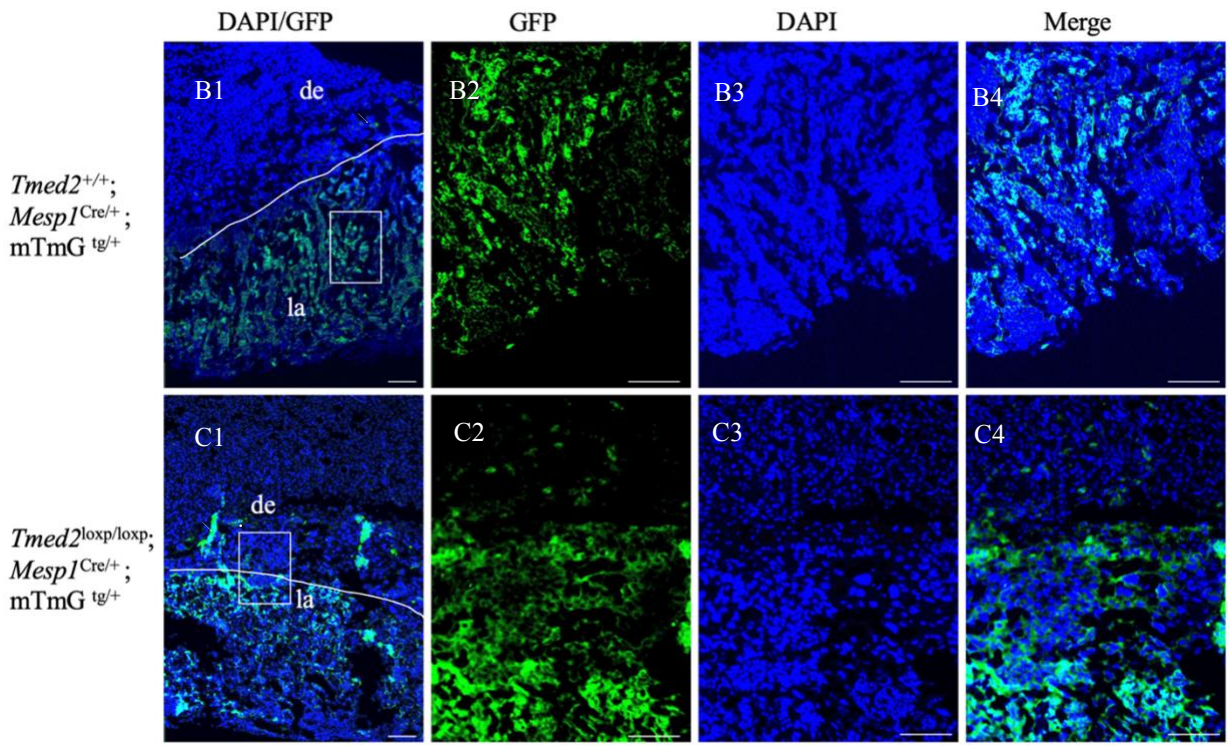

Figure 3.3 *Mesp1* derived cells are concentrated in the labyrinth layer of the placenta. (A) *Tmed2* conditional allele with LoxP sites flanking exons 2 and 3 and *Tmed2* deletion allele with Cre. Representative images stained with GFP antibody showing localization of GFP+ cells in E11.5 control (B1-B4) and mutant (C1-C4) placentas. Low magnification images (B1, C1) show the majority of GFP+ cells are within the labyrinth (la) layer of the placenta (below white line) with a few GFP+ cells within the decidua (de) and junctional zone (white arrows). High magnification of the control (B2-B4) and mutant (C2-C4) GFP+ cells showing similar regions of expression. Scale bar: 100-µm

3.4 Morphological abnormalities in the *Tmed2*$^{loxp/loxp}$; *Mesp1*$^{Cre/+}$ mutant placentas are present before embryonic death

3.4.1 A subset of Tmed2$^{loxp/loxp}$; Mesp1$^{Cre/+}$ placentas have a thin labyrinth layer at E9.5

During dissection, I found that mutant placentas at E9.5 underwent chorioallantoic attachment. Therefore, to understand whether there were morphological differences in the *Tmed2*$^{loxp/loxp}$; *Mesp1*$^{Cre/+}$ mutant placentas I used sections along with H&E staining. At E9.5, in the control placentas (n=4), the labyrinth layer and the maternal decidua are distinguishable (Fig. 3.4 A1, A2). Within the labyrinth layer of the control placenta, fetal vessels containing nucleated red blood cells and maternal sinuses with enucleated red blood cells are visible (Fig. 3.4 A3). A portion of the mutant placentas (n=3/5) appear similar to the controls with a developed labyrinth containing fetal vessels and maternal sinuses for exchange between the embryo and the mother (Fig. 3.4 B1-B3). Approximately 50% (n=2/5) of mutant placentas have a reduced thinner labyrinth layer along with fewer fetal vessels and maternal sinuses (Fig. 3.4 C1-C3). Thus, indicating variability of phenotypes in the mutant placentas at E9.5.

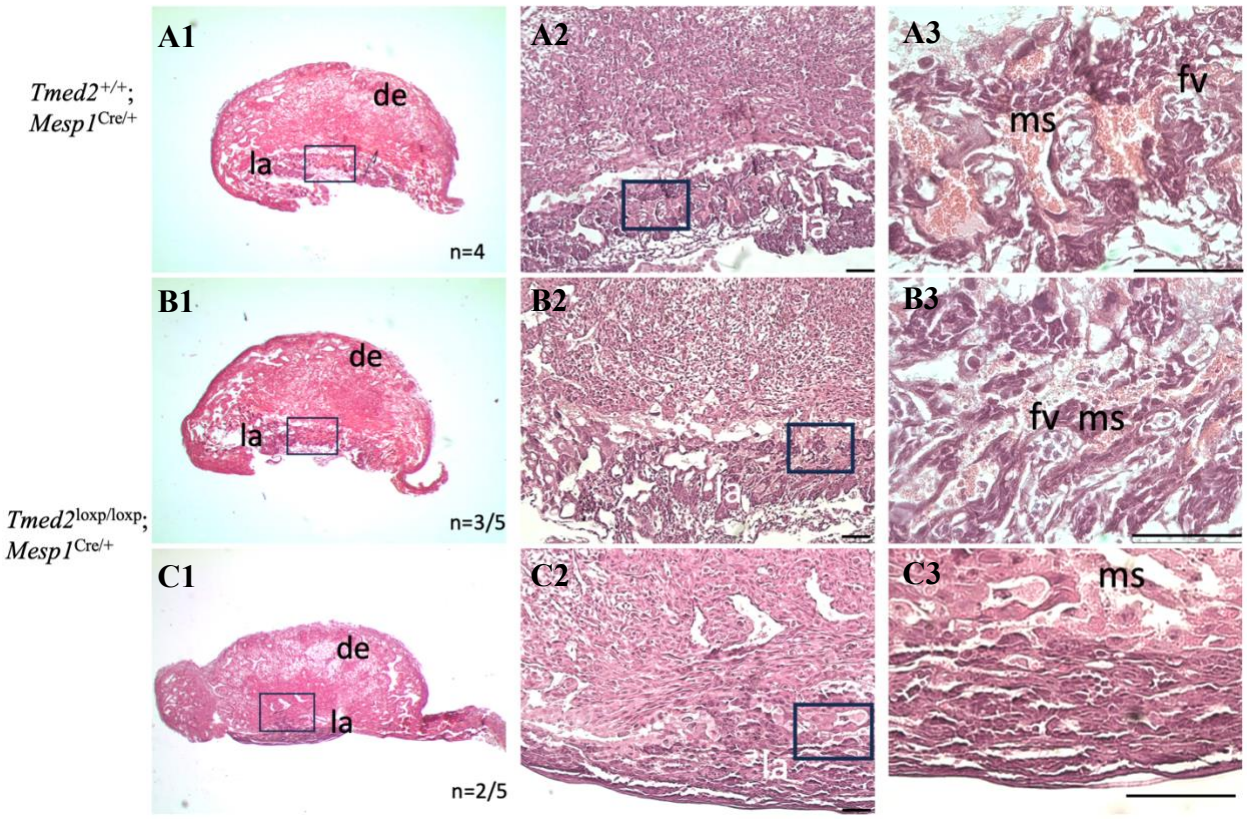

Figure 3.4. E9.5 *Tmed2*$^{loxp/loxp}$; *Mesp1*$^{Cre/+}$ placentas vary in morphological appearance.

Representative images showing the morphology of a control (A1-A3) H&E-stained E9.5 placenta and two *Tmed2*$^{loxp/loxp}$; *Mesp1*$^{Cre/+}$ placentas (B1-B3, C1-C3) The control placenta (A1) has the labyrinth layer (la) and maternal decidua (de). High magnification images within the labyrinth layer (A2, A3) display maternal sinuses (ms) with enucleated red blood cells and fetal vessels (fv) with nucleated red blood cells. Representative images (B1-B3) of a morphologically normal *Tmed2*$^{loxp/loxp}$; *Mesp1*$^{Cre/+}$ placenta containing the labyrinth layer with fetal vessels and maternal sinuses visible in the high magnification image (B3). Representative images of a *Tmed2*$^{loxp/loxp}$; *Mesp1*$^{Cre/+}$ placenta with a visibly thinner labyrinth layer (C1, C2) along with reduced vasculature at high magnification (C3). Scale bar: 100-µm

3.4.2 E10.5 Tmed2$^{loxp/loxp}$; Mesp1$^{Cre/+}$ placentas exhibit disorganized and non-uniform vessels in the labyrinth layer

I next examined the placenta morphology at E10.5 using *Bandeiraea simplicifolia* lectin 1 (BS-I) and counterstained with hematoxylin. BS-I lectin will bind to glycans, specifically N-acetylgalactosamine (DGalNAc), and will mark the fetal vasculature and decidua cells of the labyrinth placenta (Charalambous et al., 2013). In *Tmed2*$^{+/+}$; *Mesp1*$^{Cre/+}$ control placentas (n=2), the labyrinth layer is separated from the decidua by the unstained giant cells and is visible at low magnification (Fig. 3.5 A). Within the control labyrinth layer, fetal vessels are defined with dark brown staining and appear regularly spaced throughout the labyrinth layer. The fetal vessels with nucleated red blood cells are similarly sized to each other and are frequently neighboured by maternal sinuses (Fig. 3.5 A''). Mutant *Tmed2*$^{loxp/loxp}$; *Mesp1*$^{Cre/+}$ placentas (n=2) have a thinner labyrinth layer than controls (Fig. 3.5 B). The mutant labyrinth contains both fetal vessels and maternal sinuses. The distribution of the fetal vessels within the mutant labyrinth layer appears to be disorganized (Fig. 3.5 B'). The organization of maternal sinuses neighbouring fetal vessels is not as evident in the mutants. Additionally, the maternal sinuses are less frequent and thinner in comparison to the wide sinus pools in the control (Fig. 3.5 A'', B''). Therefore, we can conclude that placenta vasculature organization is disrupted in *Tmed2*$^{loxp/loxp}$; *Mesp1*$^{Cre/+}$ mutant placentas at E10.5.

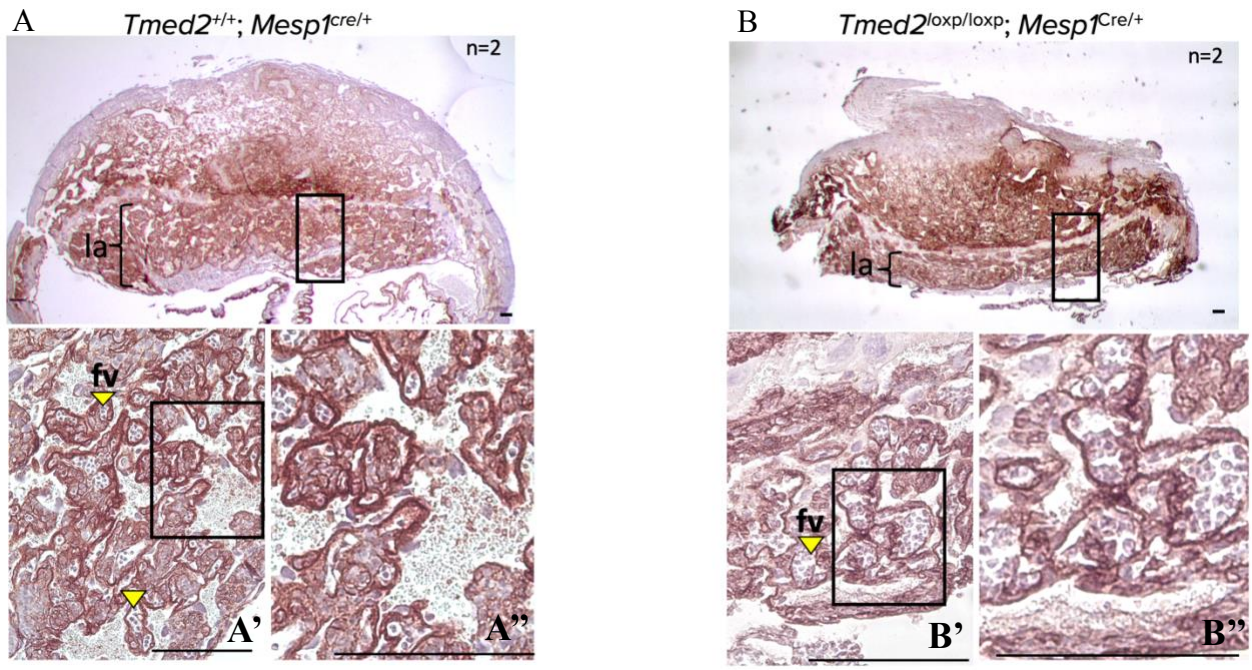

Figure 3.5. E10.5 *Tmed2*$^{loxp/loxp}$; *Mesp1*$^{Cre/+}$ placentas have irregularly distributed fetal vessels. Representative images showing the morphology of a control (A) BS-I lectin-stained E10.5 placenta and a mutant *Tmed2*$^{loxp/loxp}$; *Mesp1*$^{Cre/+}$ placenta (B). Higher magnification (A') of the boxed region of the control placenta (A) shows fetal vessel (fv/ yellow arrow) and maternal sinus distribution in the labyrinth layer. The third control image (A") shows a detailed view of the fetal vessels outlined in brown and maternal sinuses with enucleated red blood cells. Representative images display a *Tmed2*$^{loxp/loxp}$; *Mesp1*$^{Cre/+}$ placenta (B) with a thin labyrinth layer. Higher magnification image (B') shows fetal vessel and maternal sinus distribution in the labyrinth layer is less organized. The third image of the mutant (B") shows a detailed view of longer maternal sinuses and several fetal vessels that neighbour each other. Scale bar: 100-µm

3.4.3 E11.5 mutant placentas have significantly reduced labyrinth layer area and contain ectopic cells preceding the point of death at E12.5

I determined the point of death of the mutants through dissections from E9.5-E12.5. Embryonic death of the *Tmed2*$^{loxp/loxp}$; *Mesp1*$^{Cre/+}$ mutants occurs at E12.5 where embryos either had no heartbeat or were completely resorbed (Table 3.3). At E11.5, 50% of mutant embryos are dead and 50% are alive (n=7/14). Thus, I used H&E staining on placentas from live E11.5 embryos to examine the histology of the mutants before lethality.

Control placentas at E11.5 (n=4) contain various expected placental cell types including spongiotrophoblast cells and giant cells as well as fetal vessels and maternal sinuses (Fig. 3.6 A). Within the labyrinth layer there is an organized distribution of fetal vessels and a uniform size of the fetal vessels. Also, the maternal sinuses appear frequently and neighbour the fetal vessels. Mutant *Tmed2*$^{loxp/loxp}$; *Mesp1*$^{Cre/+}$ placentas (n=4) contain the same cell types as the controls (Fig. 3.6 B). However, within the labyrinth layer there are dark purple extended ectopic cells between the vessels. The shape and size of the fetal vessels appears less uniform and there is disorganization of the vessel distribution within the labyrinth tissue.

Additionally, the size of the *Tmed2*$^{loxp/loxp}$; *Mesp1*$^{Cre/+}$ labyrinth layer appears reduced compared to controls therefore I measured the area of the labyrinth layer as depicted by the green outline (Fig. 3.6 A-B). The *Tmed2*$^{loxp/loxp}$; *Mesp1*$^{Cre/+}$ mutant labyrinth layer area and ratio of labyrinth layer area compared to total area were both significantly reduced (Fig. 3.6 C, t-test, $P<0.01$). This indicates that the mutant labyrinth layer is thinner and not as extensive or expanded as the control. The decidua area, junction area and total area were not significantly different between mutants and controls (Fig. 3.6 C). The E11.5 analysis shows both quantifiable

and visual irregularities in the labyrinth layer of the *Tmed2*$^{loxp/loxp}$; *Mesp1*$^{Cre/+}$ mutant placentas before death.

Table 3.3. Genotype distribution table of live *Tmed2*$^{loxp/loxp}$; *Mesp1*$^{Cre/+}$ embryos by embryonic stage. Chi-squared test at E12.5 is statistically significant *P <0.025.

Stage	*Tmed2*$^{+/+}$; *Mesp1*$^{+/+}$	*Tmed2*$^{loxp/+}$; *Mesp1*$^{+/+}$	*Tmed2*$^{loxp/loxp}$; *Mesp1*$^{+/+}$	*Tmed2*$^{+/+}$; *Mesp1*$^{Cre/+}$	*Tmed2*$^{loxp/+}$; *Mesp1*$^{Cre/+}$	*Tmed2*$^{loxp/loxp}$; *Mesp1*$^{Cre/+}$
E9.5	13	30	6	14	15	8
E10.5	13	33	16	20	28	14
E11.5	14	27	10	16	21	7
E12.5*	9	20	7	14	18	0

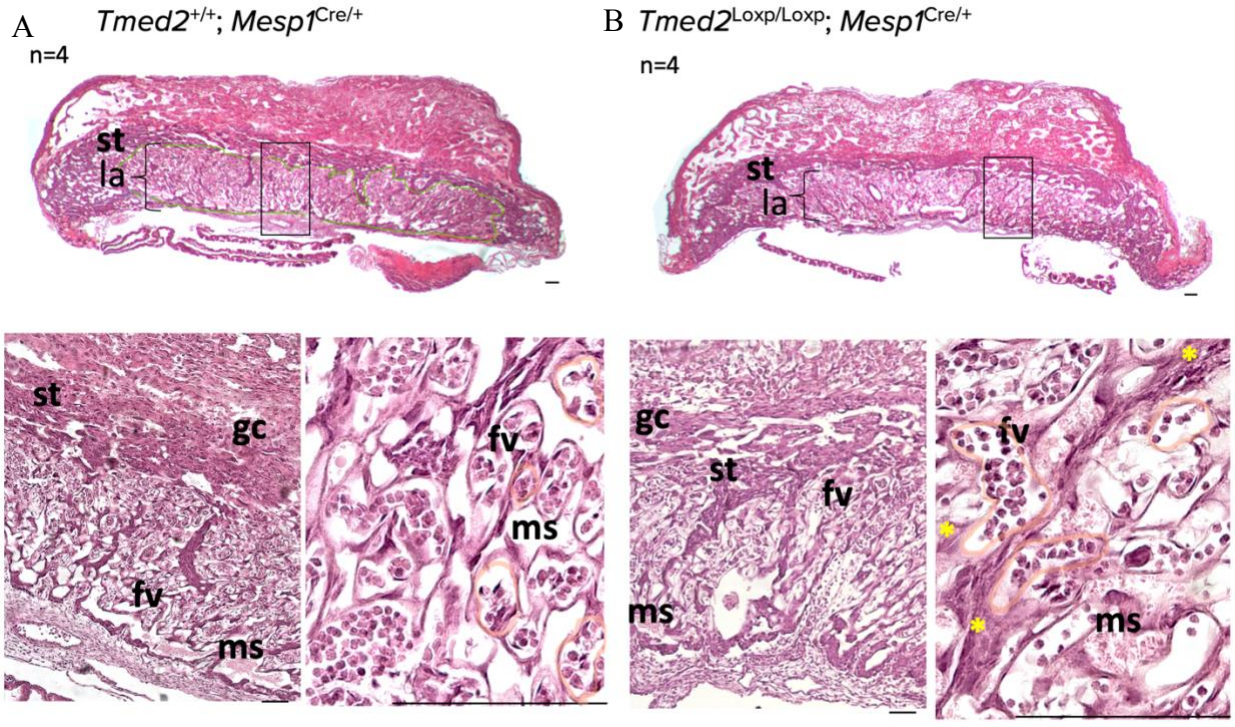

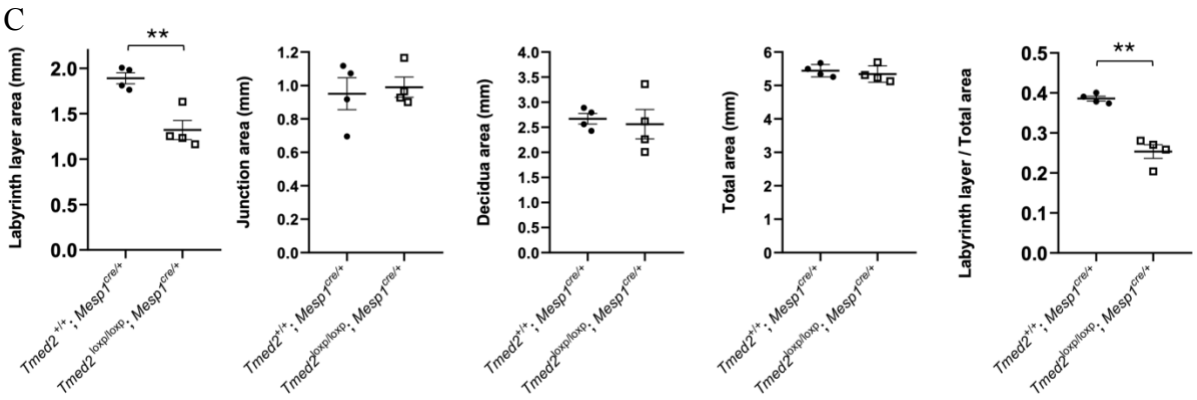

Figure 3.6. Exon 2-3 deletion of *Tmed2* in the extraembryonic mesoderm results in morphological abnormalities at E11.5 of the placenta including a thin labyrinth layer. E11.5 control (A) with high magnification images of the labyrinth (la) layer of the placenta where maternal sinuses (ms) containing enucleated red blood cells and fetal vessels (fv, orange outline) with nucleated blood cells are visible. The mutant placenta (B) displays a thinner labyrinth layer. High magnification images of the mutant labyrinth include ectopic cells (yellow stars) and disorganized vessel distribution. Labyrinth layer area (green outline) and labyrinth layer over total area is significantly reduced in mutants at E11.5 compared to controls (**P<0.01, two sample t-test) (C). Junction (includes spongiotrophoblast (st) layer and giant cells (gc)), decidua and total area are not significantly altered between mutants and controls (C). Scale bar: 100-µm

3.5 Live *Tmed2*$^{loxp/loxp}$; *Mesp1*$^{Cre/+}$ mutant embryos at E11.5 have reduced weight while placenta weight is unchanged

Embryonic weight and placental weight were measured to assess whether there were mass differences between *Tmed2*$^{loxp/loxp}$; *Mesp1*$^{Cre/+}$ mutants and controls. I took measurements from samples that were alive during dissections and found that *Tmed2*$^{loxp/loxp}$; *Mesp1*$^{Cre/+}$ mutant

embryo weight was significantly reduced (Fig. 3.7) ($p<0.01$, one-way ANOVA). Also, I measured placenta weight during dissections and found that *Tmed2*$^{loxp/loxp}$; *Mesp1*$^{Cre/+}$ mutant placenta weight was comparable to the other placenta genotypes (Fig. 3.7). This change shows that TMED2 is needed in the mesoderm to maintain normal embryo weight and possibly indicates insufficient transport to the embryo from the placenta.

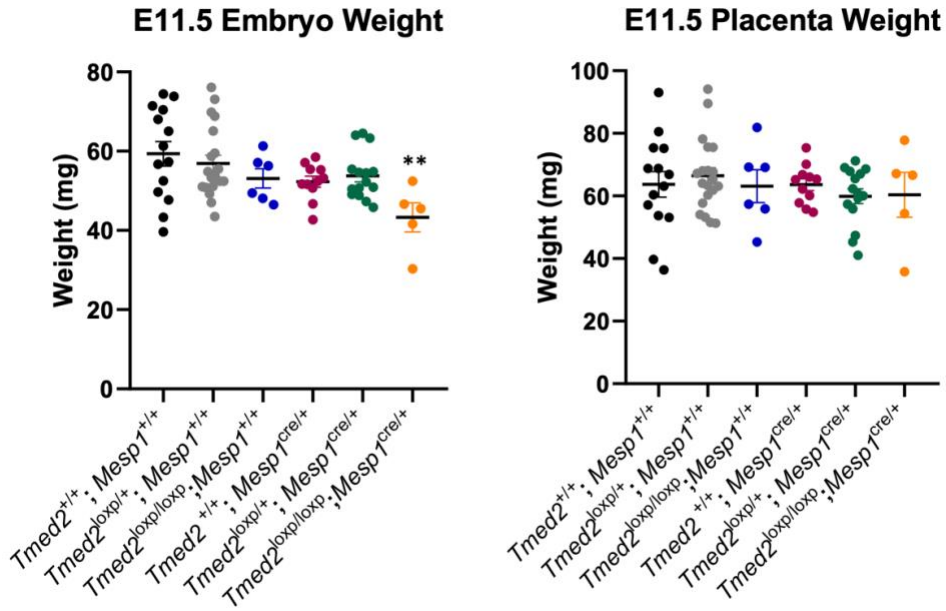

Figure 3.7. E11.5 weight comparison of *Tmed2*$^{loxp/loxp}$; *Mesp1*$^{Cre/+}$ mutant embryos and placentas. *Tmed2*$^{loxp/loxp}$; *Mesp1*$^{Cre/+}$ embryo weight (orange) is significantly reduced compared to the embryo weight of other genotypes (**$P<0.01$, One-Way ANOVA) while placenta weight is comparable.

3.6 Gene expression pattern of placental development genes are similar in mutants and controls except for the spongiotrophoblast marker *Tpbpa*

3.6.1 E9.5 Tmed2$^{loxp/loxp}$; Mesp1$^{Cre/+}$ placentas have normal expression of Pl1, SynA, SynB, Gcm1 while Tpbpa is reduced

I next used *in situ* hybridization to examine the cellular gene expression of some of the genes important for placental layer development to understand whether these regions are altered in mutants. *Pl1* (placental lactogen-1) is a prolactin expressed by trophoblast giant cells (Faria et al., 1991). At E9.5, *Pl1* was expressed in a similar number of giant cells between control and mutant *Tmed2*$^{loxp/loxp}$; *Mesp1*$^{Cre/+}$ placentas (n=4/5) (Fig. 3.8 A1, A1' + B1, B1'). *Syncytin-A* and *Syncytin-B* are envelope genes needed for trophoblast fusion to properly form the syncytiotrophoblast-I and syncytiotrophoblast-II layers (Dupressoir et al., 2011). At E9.5, *Syncytin-A* is expressed within syncytiotrophoblast-I cells of the labyrinth layer in controls and expressed in a similar number of cells in mutants (n=2) (Fig. 3.8 A2, A2' + B2, B2'). At E9.5, *Syncytin-B* is expressed within syncytiotrophoblast-II cells of the labyrinth layer in controls with a similar cellular expression pattern visible in mutants (n=4/5) (Fig. 3.8 A3, A3' + B3, B3'). There is a comparable number of cells expressing *SynA* and *SynB* in the syncytiotrophoblast bilayer between the maternal sinuses and fetal vessels of the mutant and control placentas.

Previously, in the absence of TMED2, both *Gcm1* and *Tpbpa* expression patterns were changed (Jerome-Majewska et al., 2010). *Gcm1* (glial cell missing-1) is a transcription factor that regulates *Syncytin-B* (Zhu et al., 2017). *Gcm1* is expressed by specific chorionic trophoblast cells that undergo branchpoint selection and by syncytiotrophoblast-II cells (Zhu et al., 2017). *Gcm1* expression in E9.5 control placentas is within cells of the labyrinth layer and mutant placentas (n=4/5) display a similar expression pattern (Fig. 3.8 A4, A4' + B4, B4'). The expression of *Gcm1* matches our previous histology results as we see both chorioallantoic attachment and branching occur in the *Tmed2*$^{loxp/loxp}$; *Mesp1*$^{Cre/+}$ placentas. *Tpbpa* (trophoblast specific protein

alpha) is a spongiotrophoblast cell marker and is expressed in the spongiotrophoblast cells of the control E9.5 placenta (Fig. 3.8 A5, A5') (Lawless et al., 2023). In the *Tmed2*$^{loxp/loxp}$; *Mesp1*$^{Cre/+}$ mutant placentas (n=5/5), there is expression of *Tpbpa* however, it is reduced and located in fewer cells (Fig. 3.8 B5, B5'). This indicates abnormal development of the spongiotrophoblast layer and a possible cell nonautonomous function of TMED2 based on the gene expression results observed in the mutant *Tmed2*$^{loxp/loxp}$; *Mesp1*$^{Cre/+}$ placenta.

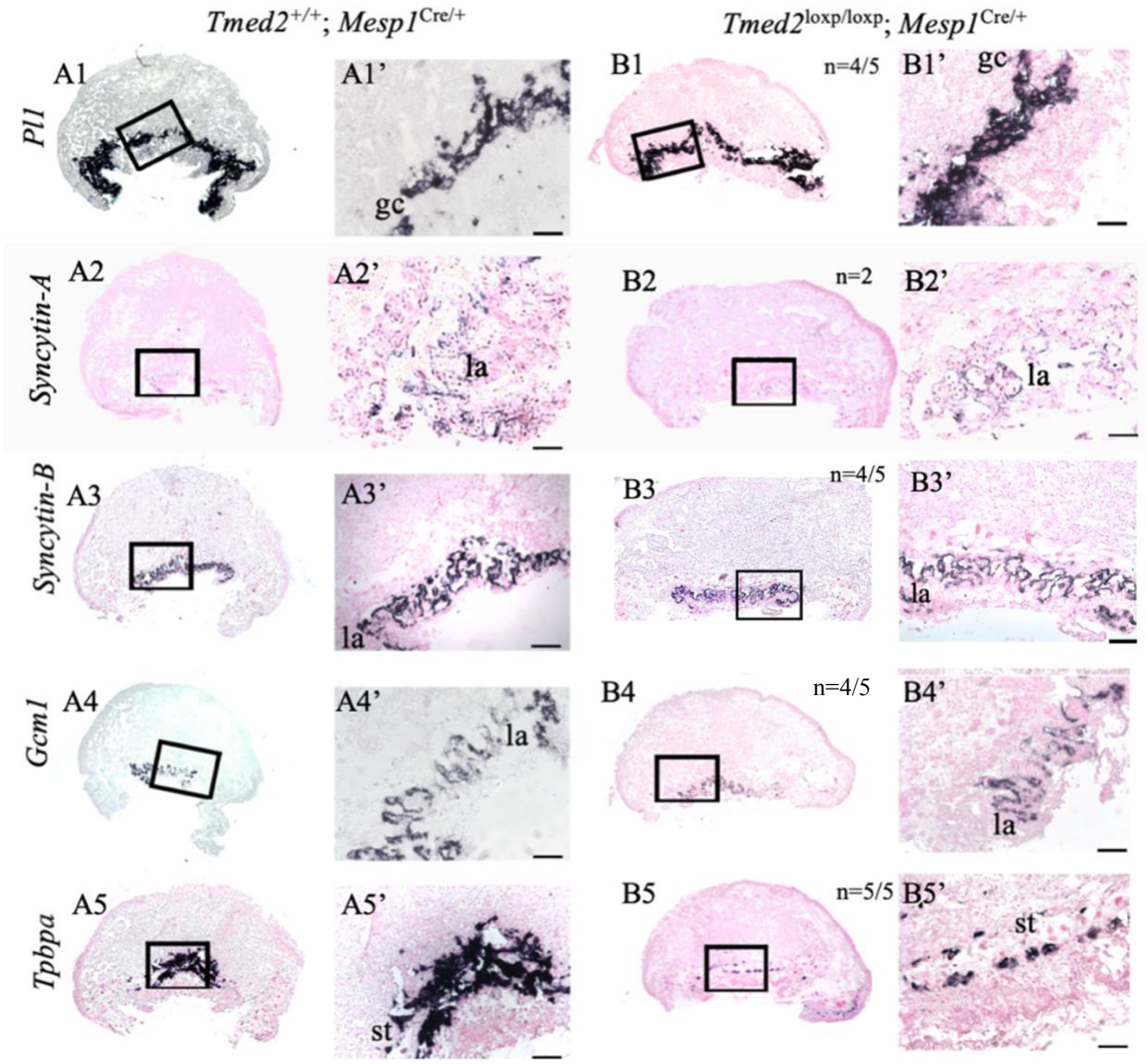

Figure 3.8. *Tpbpa* is reduced in *Tmed2*$^{loxp/loxp}$; *Mesp1*$^{Cre/+}$ placentas. Representative images of control (A1-A5) and mutant placentas (B1-B5) with *in situ* hybridization riboprobes at E9.5. *Pl1* is expressed in giant cells (gc) of control (A1, A1') and most mutants (B1, B1'). *Syncytin-A* is expressed in syncytiotrophoblast-I cells of the labyrinth in control (A2, A2') and mutant (B2, B2') placentas. *Syncytin-B* is expressed in syncytiotrophoblast-II cells of the labyrinth in control (A3, A3') and most mutant placentas (B3, B3'). *Gcm1* is expressed by chorion trophoblast cells within the labyrinth (la) in control (A4, A4') and most mutant placentas (B4, B4'). *Tpbpa* is expressed by spongiotrophoblast (st) cells above the labyrinth layer in the control placenta (A5, A5'). Expression of *Tpbpa* is present but reduced and restricted to fewer cells in all mutant placentas (B5, B5'). Scale bar: 100-µm

3.6.2 E11.5 Tmed2$^{loxp/loxp}$; Mesp1$^{Cre/+}$ placentas have normal expression of Pl1, SynB, Gcm1 while Tpbpa is reduced

I next examined the gene expression patterns of *Pl1, Gcm1, SynB* and *Tpbpa* using *in situ* hybridization at E11.5 to determine if there were any changes in the expression before embryonic death. At E11.5, *Pl1* is expressed throughout the trophoblast giant cells in a layer between the decidua and spongiotrophoblasts in both control and *Tmed2*$^{loxp/loxp}$; *Mesp1*$^{Cre/+}$ placentas (n=1) (Fig. 3.9 A1, A1' + B1, B1'). *Gcm1* expression is widespread in chorionic trophoblast cells in control and *Tmed2*$^{loxp/loxp}$; *Mesp1*$^{Cre/+}$ mutants at E11.5 (n=1) (Fig. 3.9 A2, A2' + B2, B2'). *Syncytin-B* expression is spread throughout cells of the labyrinth layer, specifically in similar numbers of syncytiotrophoblast-II cells, in control and *Tmed2*$^{loxp/loxp}$; *Mesp1*$^{Cre/+}$ mutants at E11.5 (n=3) (Fig. 3.9 A3, A3' + B3, B3'). *Tpbpa* expression at E11.5 is in the spongiotrophoblast

cells of the control placenta in a thick layer of cells (Fig. 3.9 A4, A4'). *Tpbpa* expression in *Tmed2*$^{loxp/loxp}$; *Mesp1*$^{Cre/+}$ mutant placentas is present but appears in a smaller layer and fewer cells in comparison to the control placenta (n=3) (Fig. 3.9 B4, B4'). Therefore, *Tpbpa* continues to have less expression in mutant placentas at E11.5 indicating a possible restriction of the spongiotrophoblast cell layer. Additionally, at E11.5, there was no significant reduction of junctional zone area in mutants which is possibly due to improper differentiation of the spongiotrophoblast cells leading to reduced *Tpbpa* expression without a change in the area (Fig. 3.6 C).

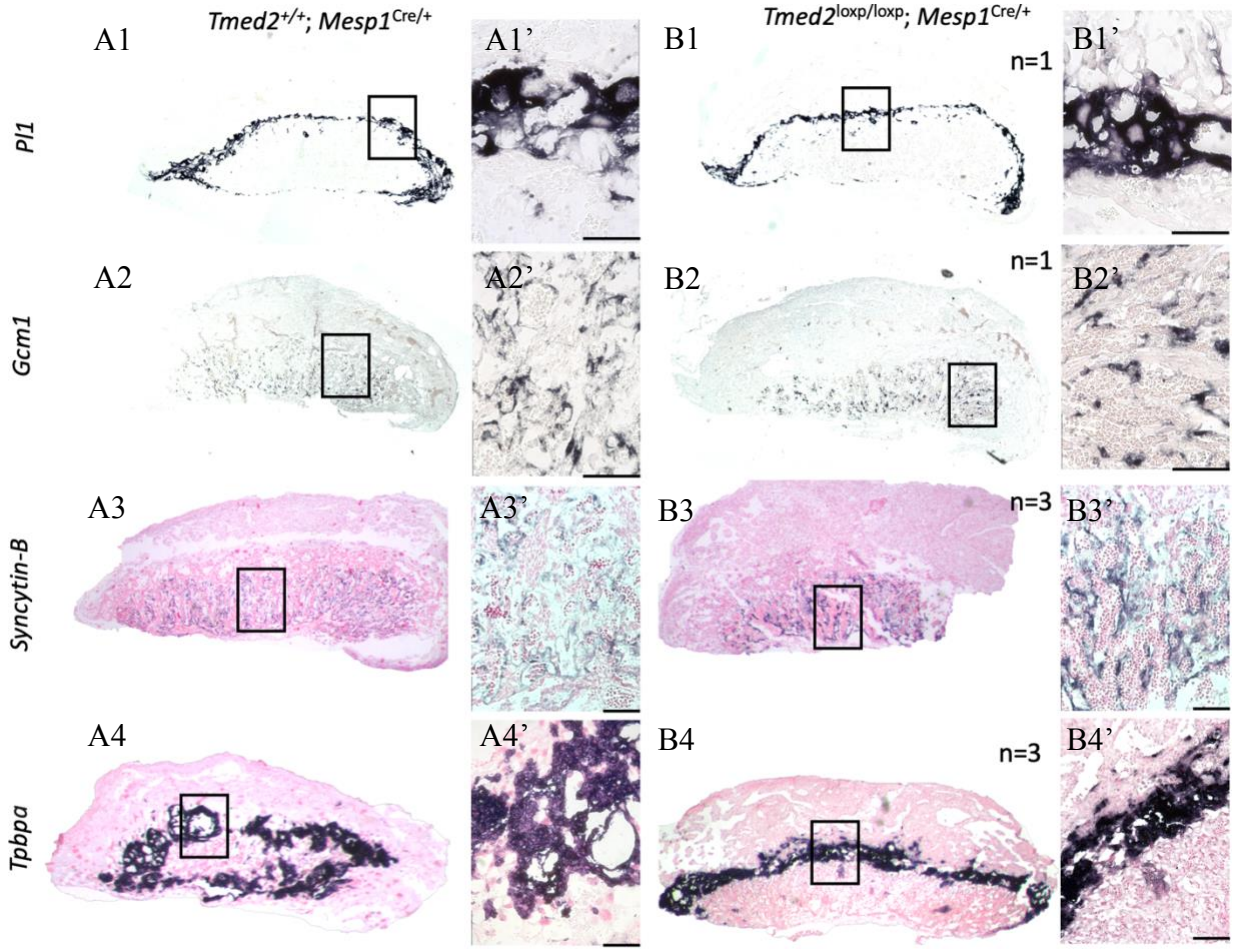

Figure 3.9. E11.5 placental gene expression in control and *Tmed2*$^{loxp/loxp}$; *Mesp1*$^{Cre/+}$ placentas. Control (A1-A4) and mutant (B1-B4) placentas with *in situ* hybridization riboprobes

at E11.5. *Pl1* is expressed in giant cells of control (A1, A1') and mutant (B1, B1') placentas. *Gcm1* is expressed by chorion trophoblast cells in control (A2, A2') and mutant (B2, B2') placentas. *Syncytin-B* is expressed in syncytiotrophoblast-II cells in control (A3, A3') and mutant (B3, B3') placentas. *Tpbpa* is expressed in spongiotrophoblast cells in the control placenta (A4, A4') and *Tpbpa* is present yet decreased in mutants (B4, B4'). Scale bar: 100-µm

3.7 *Tmed2*$^{loxp/loxp}$; *Mesp1*$^{Cre/+}$ mutant placentas have abnormal protein localization

3.7.1 Fibronectin expression is increased, more fibrillar and cellularly retained in Tmed2$^{loxp/loxp}$*; Mesp1*$^{Cre/+}$ *placentas*

Fibronectin is an extracellular matrix protein that binds integrins, aids cell adhesion and is found in the placenta (Hsiao et al., 2017; Saylam et al., 2002; Singh et al., 2010). Previously, fibronectin was retained in the *Tmed2*$^{99J/99J}$ placenta mutant model and identified as a TMED2 cargo (Hou & Jerome-Majewska, 2018). Therefore, we wanted to determine if there were changes in the expression of a previously known TMED2 cargo protein in the *Tmed2*$^{loxp/loxp}$; *Mesp1*$^{Cre/+}$ mutant placentas. In control placentas (n=2), I examined fibronectin protein distribution within the labyrinth layer of the placenta since it is secreted by endothelial cells (Luo & Jian, 2023). In controls, fibronectin is expressed as strands around groups of nucleated cells, surrounding the fetal vessels lined by endothelial cells, and appears arranged (Fig. 3.10 A1-A4). In *Tmed2*$^{loxp/loxp}$; *Mesp1*$^{Cre/+}$ mutant placentas (n=3), fibronectin expression is increased, and the distribution of this protein appears more fibrillar and less arranged (Fig. 3.10 B1-B4). Also, there is visible overlap with the nucleated cells of the placenta and there is a loss of uniformity indicating a change in fibronectin protein localization or secretion by the endothelial cells.

Furthermore, I used KDEL and fibronectin co-immunofluorescence to determine the cellular localization of fibronectin (Fig. 3.11). KDEL is an amino acid sequence located on resident ER proteins and it can be used to investigate whether proteins are localized to the ER (Cela et al., 2022). In control placentas at E9.5 (n=2), there is expression of both fibronectin and KDEL in the labyrinth layer with some co-localization and other regions without co-localization (Fig. 3.11 A1-A4). This indicates at this timepoint there is likely some fibronectin in the ER that is in the process of being secreted outside of the cells in addition to fibronectin in the extracellular matrix. *Tmed2*$^{loxp/loxp}$; *Mesp1*$^{Cre/+}$ mutant placentas at E9.5 (n=2) contain increased expression of both fibronectin and KDEL in the labyrinth layer (Fig. 3.11 B1-B4). Fibronectin expression in the mutant placenta appears to be co-expressed with KDEL with more co-localization than the control placenta. This indicates that fibronectin is retained in the ER of mutant placentas. Therefore, based on these results we can conclude that TMED2 is needed in the extraembryonic mesoderm for normal expression, secretion and localization of fibronectin by the placenta endothelial cells.

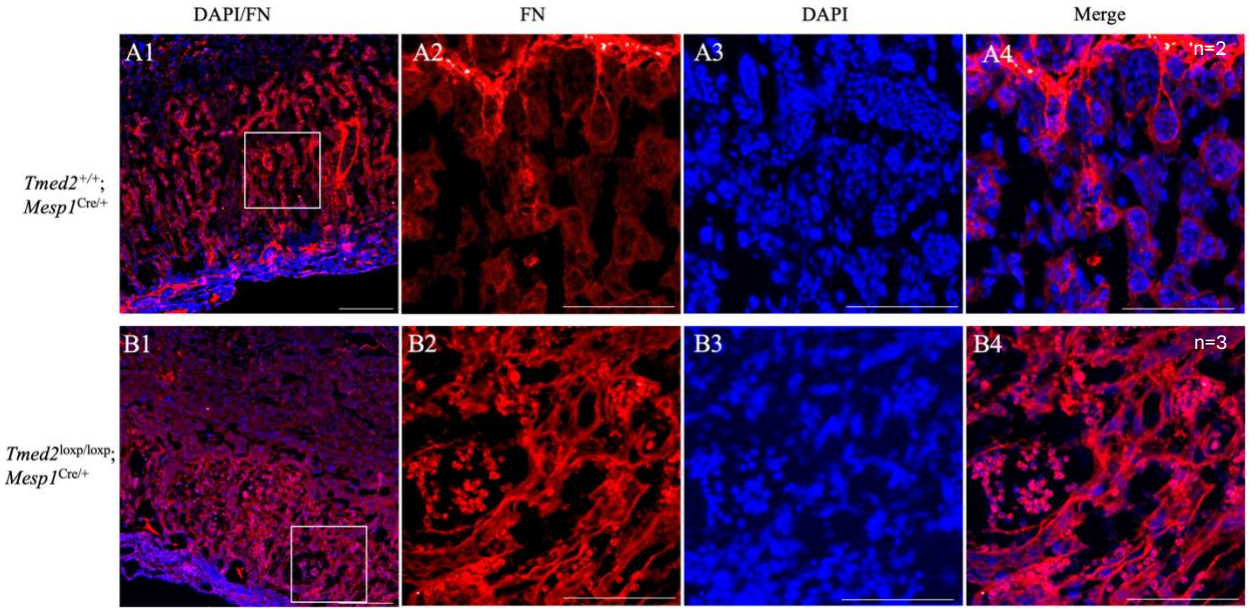

Figure 3.10. Fibronectin protein is increased and the pattern of expression is changed in *Tmed2*$^{loxp/loxp}$; *Mesp1*$^{Cre/+}$ mutant placentas. Representative images showing fibronectin localization in control (A1-A4) and mutant placentas (B1-B4) at E11.5. High magnification images within the labyrinth layer of the placenta (A2-A4) displays fibronectin surrounding groups of nucleated cells. Fibronectin expression in mutant placentas appears increased with longer extended fibres and expression in nucleated cells shown in the high magnification images of the labyrinth layer (B2-B4). Scale bar: 100-µm

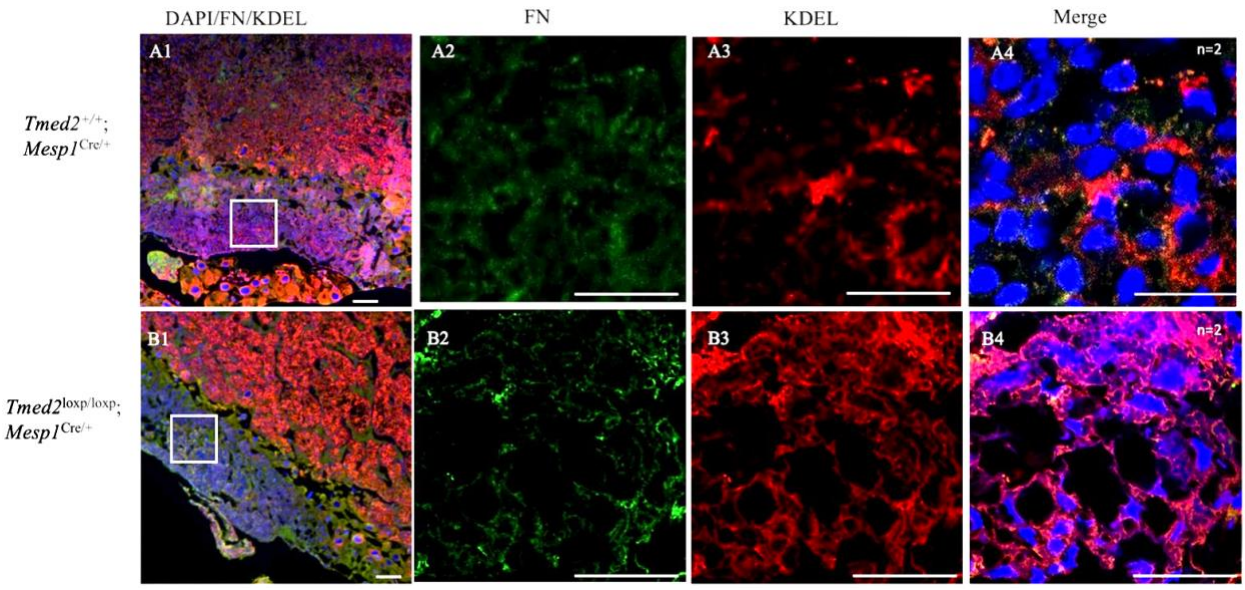

Figure 3.11 Fibronectin and KDEL expression and co-localization are increased in *Tmed2*$^{loxp/loxp}$; *Mesp1*$^{Cre/+}$ mutant placentas. Representative images showing fibronectin and KDEL protein distribution in control (A1-A4) and mutant placentas (B1-B4) at E9.5. High magnification images within the labyrinth layer of the placenta (A2-A4) displays fibronectin and KDEL surrounding nucleated cells. Fibronectin and KDEL expression and regions of co-expression are both increased in *Tmed2*$^{loxp/loxp}$; *Mesp1*$^{Cre/+}$ mutant placentas (B2-B4). Scale bar: 100-µm

3.7.2 ITGA4 receptor expression is altered while the ligand VCAM1 is normally expressed in Tmed2$^{loxp/loxp}$; Mesp1$^{Cre/+}$ placentas

To continue to examine protein expression by the placenta endothelial cells, I examined an adhesion molecule, vascular cell adhesion molecule-1 (VCAM1), which was previously identified as a potential protein cargo of TMED2 as it was incorrectly localized in the absence of TMED2 (Hou & Jerome-Majewska, 2018; Kong et al., 2018). Additionally, VCAM1 will bind to the receptor, integrin alpha-4 (ITGA4), this receptor is a binding partner of fibronectin that we found to be mislocalized in the *Tmed2*$^{loxp/loxp}$; *Mesp1*$^{Cre/+}$ placentas (Fig. 3.10 B1-B4) (Wu, 1997; Wu et al., 1995). Therefore, I examined the protein expression using immunofluorescence at E11.5 of ITGA4 and VCAM1 to understand whether the mesoderm specific deletion of TMED2 leads to their mislocalization at the syncytiotrophoblast and endothelial cells. ITGA4 protein expression in control placentas (n=2) is found in an organized pattern within the labyrinth layer tissue (Fig. 3.12 A1). At high magnification, ITGA4 encircles groups of nucleated cells and appears to be localized to a single layer of trophectoderm-derived cells (Fig. 3.12 A2-A4). In *Tmed2*$^{loxp/loxp}$; *Mesp1*$^{Cre/+}$ placentas (n=3), ITGA4 does not appear to be as organized in the labyrinth layer (Fig. 3.12 B1). At high magnification, ITGA4 expression is not found in a single layer surrounding the nucleated cells (Fig. 3.12 B2-B4). Some of the ITGA4 expression appears to be around groups of nucleated cells like the controls but a lot of ITGA4 expression overlaps with the nucleated cells and has lost the organized pattern. Next, I examined VCAM1 in the labyrinth layer of control placentas (n=2) where it surrounds groups of nucleated cells where fetal vessels are expected and appears to be expressed in a singular layer (Fig. 3.12 C1-C4).

Similarly, in *Tmed2*$^{loxp/loxp}$; *Mesp1*$^{Cre/+}$ placentas (n=3), VCAM1 expression by the endothelial cells appears in a single layer around the fetal vessels and resembles the expression pattern of the control placentas (Fig. 3.12 D1-D4). To conclude, TMED2 is not required in the extraembryonic mesoderm for normal VCAM1 transport and localization but it is needed in these cells for normal ITGA4 expression. This indicates the lack of TMED2 in mesoderm-derived cells may be impacting protein transport to the syncytiotrophoblast cell surface. Additionally, there are possibly other mechanisms or proteins allowing normal VCAM1 protein transport at the endothelial cell surface.

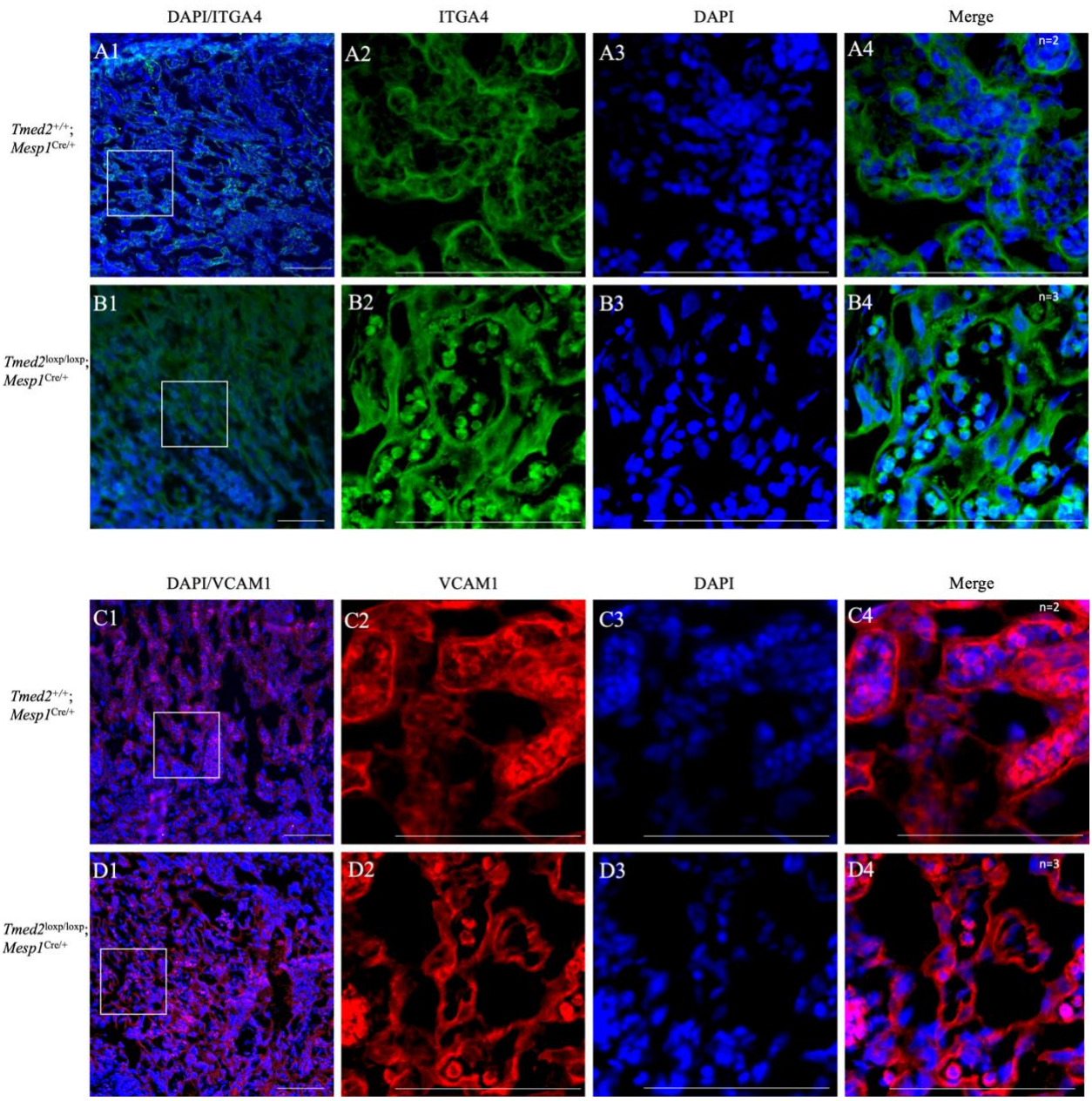

Figure 3.12. Integrin alpha-4 expression is altered in *Tmed2*$^{loxp/loxp}$; *Mesp1*$^{Cre/+}$ placentas while VCAM1 expression pattern remains the same. Representative images showing ITGA4 localization in control (A1-A4) and mutant placentas (B1-B4) at E11.5. High magnification images within the labyrinth layer of the placenta (A2-A4) displays integrin alpha-4 in a uniform tissue pattern on trophoblast cells around groups of nucleated cells. Integrin alpha-4 in mutant placentas is not localized in a uniform pattern and appears spread throughout the cells (B2-B4).

Representative images showing VCAM1 localization in control (C1-C4) and mutant placentas (D1-D4) at E11.5. High magnification images within the labyrinth layer of the placenta (C2-C4) shows VCAM1 expression pattern by the endothelial cells which is similar to the mutant (D2-D4) high magnification images. Scale bar: 100-µm

3.7.3 MCT1 and MCT4 protein expression changes in E10.5 Tmed2$^{loxp/loxp}$; Mesp1$^{Cre/+}$ mutant placentas

Next, to examine the syncytiotrophoblast bilayer that separates maternal sinuses and fetal vessels, I analyzed the monocarboxylate transporter proteins that are located there (Nadeau & Charron, 2014). Monocarboxylate transporters, MCT1 and MCT4, are localized to the cell membrane and will transport lactate and other monocarboxylates (Nagai et al., 2010). MCT1 is expressed at the syncytiotrophoblast-I layer and MCT4 is localized to the syncytiotrophoblast-II layer of the mouse placenta (Nadeau & Charron, 2014; Nagai et al., 2010). Therefore, to examine protein expression at the syncytiotrophoblast bilayer at E10.5, I used these two proteins. In the labyrinth layer of control placentas (n=2), both MCT1 and MCT4 expression are visible (Fig. 3.13 A1). Where the syncytiotrophoblast bilayer is expected to form, MCT1 and MCT4 expression mirror each other and form a polarized bilayer without co-expression (Fig. 3.13 A2-A4). In some *Tmed2*$^{loxp/loxp}$; *Mesp1*$^{Cre/+}$ mutant placentas (n=1/4), the polarized syncytiotrophoblast bilayer is visible based on the expression of MCT1 and MCT4 (Fig. 3.13 B1-B4). However, MCT1 and MCT4 expression appear to be marginally decreased compared to controls. In the majority of *Tmed2*$^{loxp/loxp}$; *Mesp1*$^{Cre/+}$ mutant placentas that I examined (n=3/4), syncytiotrophoblast-I cells express less MCT1 (Fig. 3.13 C2) while MCT4 expression appears

thicker indicating that it may not be localized to only the syncytiotrophoblast-II membrane (Fig. 3.13 C3). In these mutants, there is a loss of polarization of protein expression at the syncytiotrophoblast bilayer and there is no longer normal MCT1 and MCT4 localization (Fig. 3.13 C1-C4). We can conclude that the syncytiotrophoblast bilayer may require TMED2 in the extraembryonic mesoderm at E10.5 for normal transport or organization of proteins such as MCT1 and MCT4.

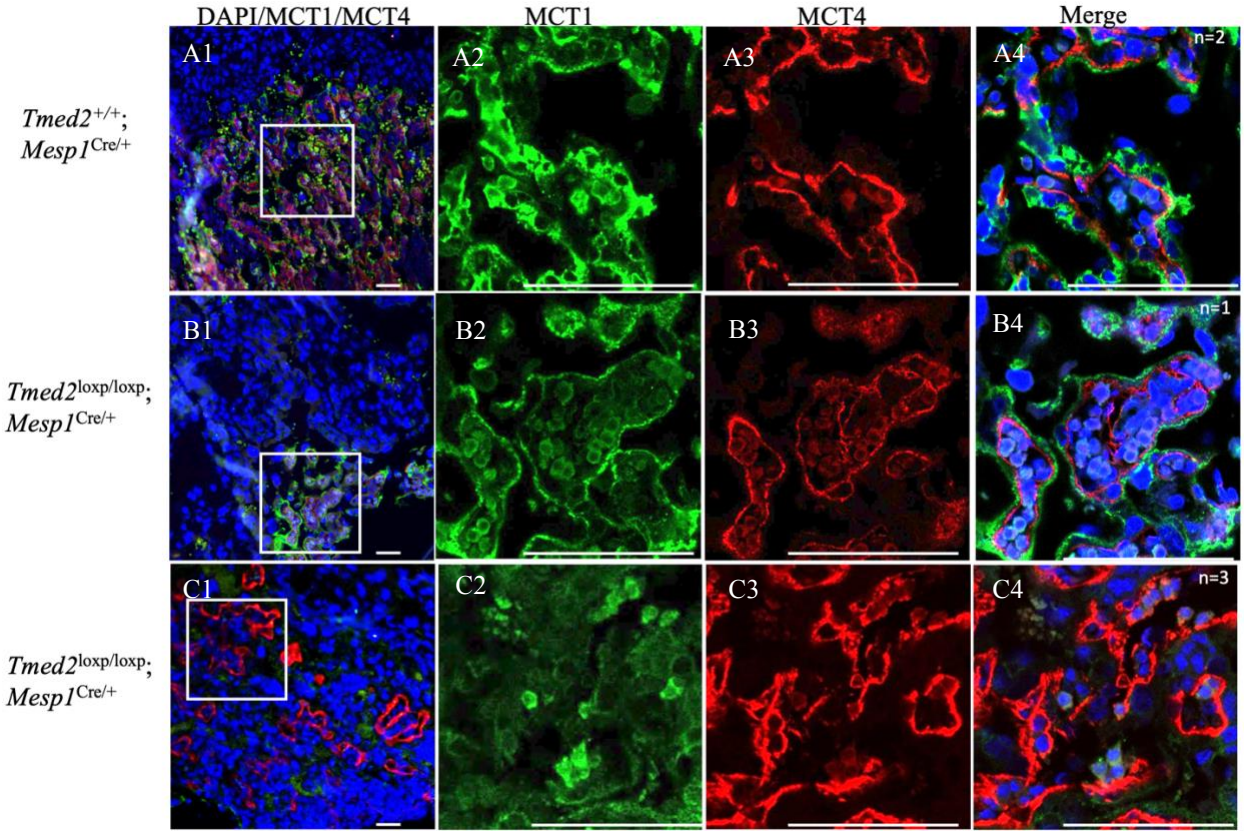

Figure 3.13. E10.5 MCT1 expression is decreased and MCT4 expression is increased while polarization is absent in *Tmed2*$^{loxp/loxp}$; *Mesp1*$^{Cre/+}$ placentas. Representative images showing MCT1 and MCT4 localization in control (A1-A4) and two mutant placentas (B1-B4, C1-C4) at E10.5. High magnification images (A2-A4) within the labyrinth layer of the control placenta

shows MCT1 and MCT4 defining the syncytiotrophoblast bilayer with neighbouring expression around the labyrinth vessels. High magnification images show one mutant placenta where MCT1 expression is slightly decreased and less continuous (B2) while the merge image (B4) displays continued polarization of MCT1 and MCT4. Representative high magnification images of most mutant placentas (C2-C4) show a decrease of MCT1 expression (C2) while MCT4 expression is increased and has a thicker region of expression. Additionally, the polarization of MCT1 and MCT4 is absent (C4). Scale bar: 50-µm (A1, B1, C1) and 100-µm (A2-A4, B2-B4, C2-C4)

3.7.4 MCT1 and MCT4 proteins are incorrectly expressed in a minority of E11.5 Tmed2$^{loxp/loxp}$; Mesp1$^{Cre/+}$ mutant placentas

I next examined protein expression at the syncytiotrophoblast bilayer at E11.5 by using MCT1 and MCT4 to continue to understand whether these proteins are correctly localized in the *Tmed2*$^{loxp/loxp}$; *Mesp1*$^{Cre/+}$ mutant placentas. Control placentas (n=2) at E11.5 have the same expression pattern of MCT1 and MCT4 as the E10.5 control placentas where a polarized bilayer is visible (Fig. 3.14 A1-A4). The majority (n=2/3) of E11.5 *Tmed2*$^{loxp/loxp}$; *Mesp1*$^{Cre/+}$ mutants that I examined contained normal expression of MCT1 and MCT4 in the labyrinth layer of the placenta (Fig. 3.14 B1-B4). One E11.5 *Tmed2*$^{loxp/loxp}$; *Mesp1*$^{Cre/+}$ mutant placenta has less polarization of MCT1 and MCT4 and some co-expression (Fig. 3.14 C1-C4). This indicates that there is variability of MCT1 and MCT4 protein expression and localization in the *Tmed2*$^{loxp/loxp}$; *Mesp1*$^{Cre/+}$ mutants. At both E11.5 and E10.5, some mutants appear to have normal protein localization at the syncytiotrophoblast bilayer while others have incorrect protein localization.

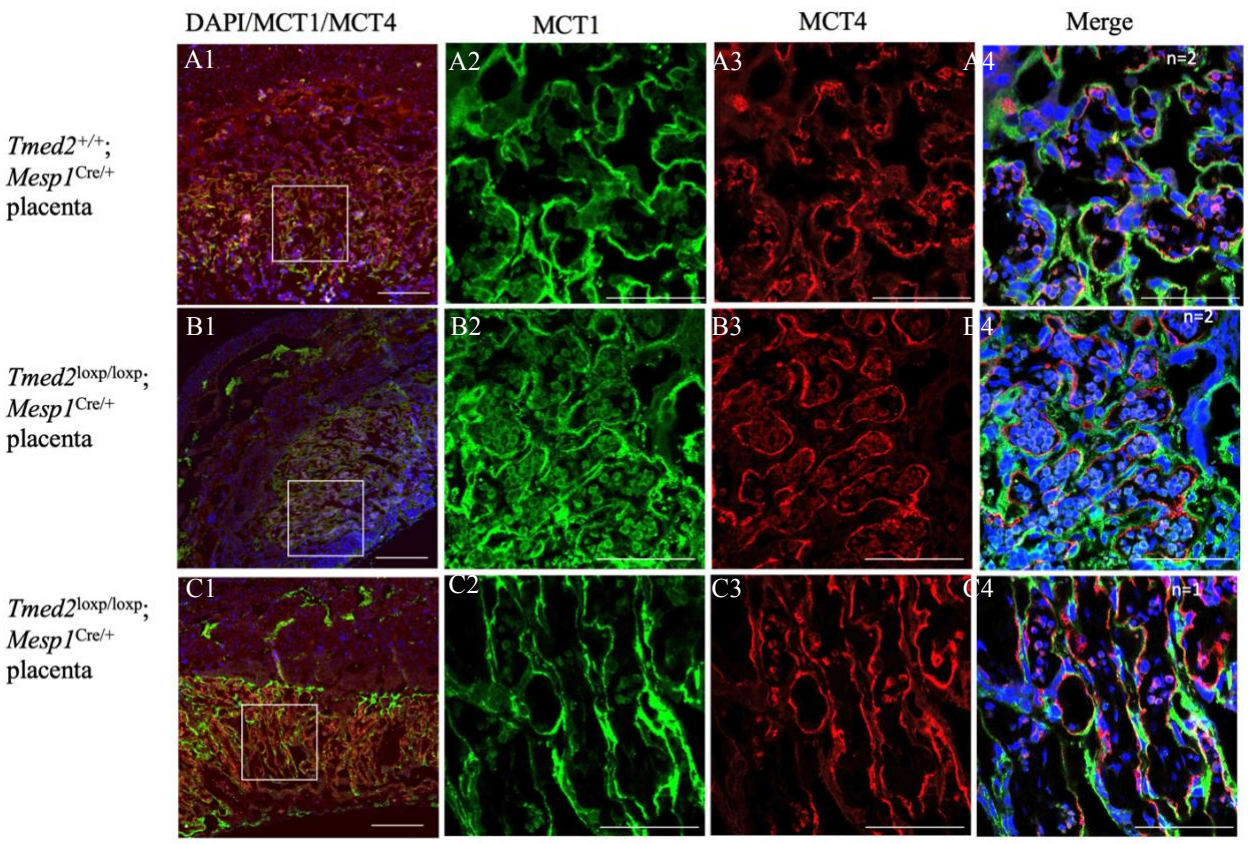

Figure 3.14. MCT1 and MCT4 expression remains similar in 2/3 *Tmed2*$^{loxp/loxp}$; *Mesp1*$^{Cre/+}$ placentas at E11.5. Representative images showing MCT1 and MCT4 localization in control (A1-A4) and two mutant placentas (B1-B4, C1-C4) at E11.5. High magnification images (A2-A4) within the labyrinth layer of the control placenta shows MCT1 and MCT4 polarization. Similarly, representative high magnification images of a mutant placenta display a similar expression pattern of MCT1 and MCT4 (B2-B4). One mutant placenta (C1) contains non-continuous expression of both MCT1 (C2) and MCT4 (C3) while polarization is absent in certain regions (C4). Scale bar: 100µm

3.8 CD31 expression remains the same in *Tmed2*$^{loxp/loxp}$; *Mesp1*$^{Cre/+}$ placentas at E11.5

To further examine protein expression in the endothelial cells lining the fetal vessels of the placentas, I used CD31 (cluster of differentiation 31 or PECAM1), an endothelial cell marker (Lertkiatmongkol et al., 2016; Tai-Nagara et al., 2017). In the labyrinth layer of control placentas (n=2), CD31 expression appears in a single layer around the groups of nucleated cells, fetal vessels, in a repetitive round pattern (Fig. 3.15 A1-A4). In *Tmed2*$^{loxp/loxp}$; *Mesp1*$^{Cre/+}$ mutant placentas (n=3), endothelial cell expression of CD31 in the placental labyrinth appears similar to controls (Fig. 3.15 B1-B4). CD31 is expressed in an organized distribution around the nucleated cells where fetal vessels are expected. Therefore, expression of CD31 by endothelial cells does not require TMED2 in the extraembryonic mesoderm for normal localization and it is likely not a cargo protein of TMED2.

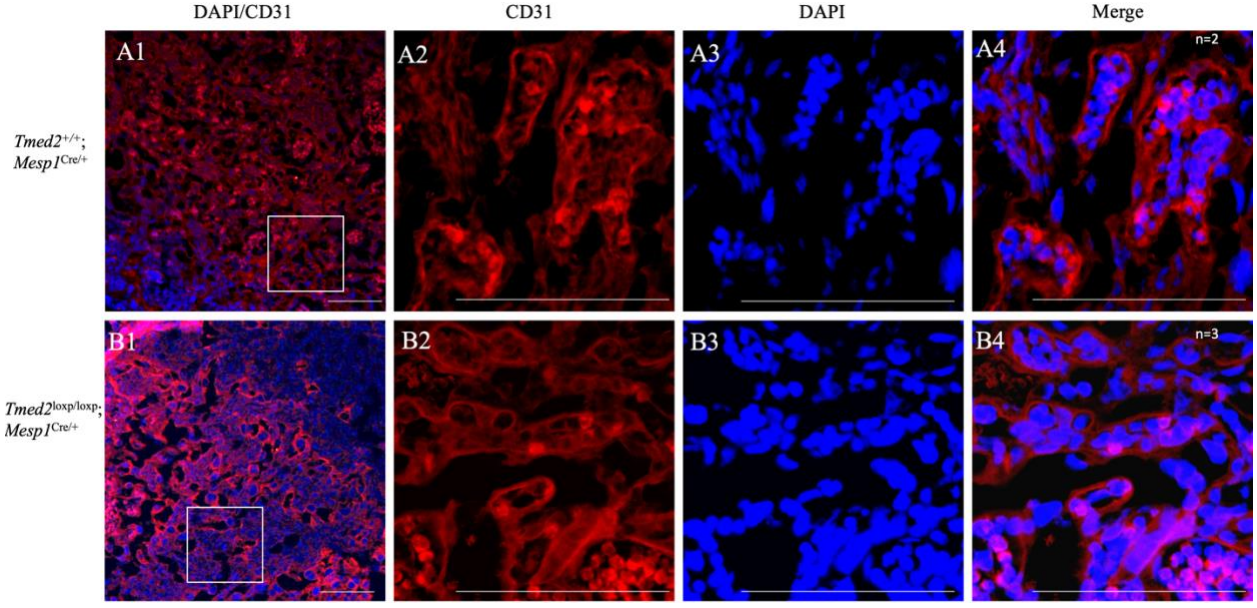

Figure 3.15. CD31 is expressed in E11.5 *Tmed2*$^{loxp/loxp}$; *Mesp1*$^{Cre/+}$ placentas. Representative images showing CD31 localization in control (A1-A4) and mutant placentas (B1-B4) at E11.5.

High magnification images within the labyrinth layer of the placenta (A2-A4) contain CD31 expression around groups of nucleated cells in a single layer where the endothelial cells of the fetal vessels are located. Mutant placentas CD31 expression appears similar to controls at high magnification where CD31 is expressed surrounding nucleated cells in a single layer. Scale bar: 100-µm

CHAPTER IV: DISCUSSION

TMED2 is an essential protein for normal murine embryonic and placental development (Jerome-Majewska et al., 2010). My project aimed to further understand the functional role and requirement of TMED2 in placenta development. The previous analysis of TMED2 in the placenta was done in vivo using a missense mutation where TMED2 was removed from the entire placenta (Jerome-Majewska et al., 2010). TMED2 was also examined in an explant model and removed in a tissue-specific manner (Hou & Jerome-Majewska, 2018). Here, my aim was to investigate the cell-type-specific function of TMED2 using Cre-LoxP recombination to remove TMED2 from the extraembryonic mesoderm of the placenta.

4.1 The exon 2-3 deletion of *Tmed2* leads to developmental delay and earlier arrest than the missense 99J mutation

To first examine my hypothesis, we phenotypically characterized a new homozygous exon 2-3 deletion of *Tmed2* that we planned to use conditionally in a cell-type-specific manner in the later aim. This mutation was used as we are unable to conditionally delete TMED2 with the previous 99J missense mutation model. We found that similarly to the 99J mutation, this deletion leads to abnormal embryonic and placental development, as expected. However, these embryos arrested by E8.5 and were more developmentally delayed. This is a more severe mutation in comparison to the *Tmed2*$^{99J/99J}$ mutants that arrest by E11.5 (Jerome-Majewska et al., 2010). There was no embryonic TMED2 protein observed in the *Tmed2*$^{99J/99J}$ mutants however, this may be a hypomorphic allele that creates a partial loss of function (Baker, 2011; Jerome-Majewska et al., 2010). Possibly, TMED2 protein is still generated and went undetected due to antibody specificity thus explaining the severity of the exon 2-3 deletion of *Tmed2* that we used here.

Although this *Tmed2*$^{-/-}$ mutation differs from that of the *Tmed2*$^{99J/99J}$ mutants, we were able to observe that this deletion of TMED2 creates embryonic delay and prevents proper embryo and placenta development. Therefore, we used this deletion of *Tmed2*, in the extraembryonic mesoderm, to examine our hypothesis of whether TMED2 is required in the extraembryonic mesoderm for placental labyrinth layer development.

4.2 The labyrinth layer forms in the absence of TMED2 in the extraembryonic mesoderm

Initially, I hypothesized that TMED2 would be required in the extraembryonic mesoderm for labyrinth layer formation. Yet, *Tmed2*$^{loxp/loxp}$; *Mesp1*$^{Cre/+}$ mutant placentas exhibit labyrinth layer formation at all embryonic stages. Hence, it is likely the presence of TMED2 in the chorionic ectoderm is sufficient for chorioallantoic attachment to occur and for labyrinth layer formation. In the previous explant model where TMED2 was absent in the extraembryonic mesoderm-derived allantois, attachment and reduced fusion was observed (Hou & Jerome-Majewska, 2018). This shows that attachment still occurs in the absence of TMED2 in some of the extraembryonic mesoderm-derived tissues. Yet, when TMED2 was absent in the partially extraembryonic mesoderm-derived (chorionic mesothelium) and partially extraembryonic ectoderm-derived chorion, fusion never occurs, and attachment fails in 50% of the sample (Hou & Jerome-Majewska, 2018). From our results and the previous explant studies, we can conclude that TMED2 is not needed in the extraembryonic mesoderm of the chorion or allantois for labyrinth layer formation.

4.3 TMED2 is needed in the extraembryonic mesoderm for normal placenta development

Although I found that chorioallantoic attachment and fusion occur in the absence of TMED2 in the extraembryonic mesoderm, I observed other abnormalities in the placenta. This suggests the requirement of TMED2 in the extraembryonic mesoderm for normal placenta development. I found a thin labyrinth layer in the mutants beginning in some placentas at E9.5 and in all placentas by E11.5. A small labyrinth layer has been previously found in mutant mouse models and reduces the area of functional exchange between the embryo and the mother which, is needed for continued development (Woods et al., 2018; Yung et al., 2012). Fetal-maternal exchange is likely reduced in the *Tmed2*$^{loxp/loxp}$; *Mesp1*$^{Cre/+}$ mutants since the smaller labyrinth placental area coincided with significantly decreased embryonic weight. Additionally, the labyrinth layer is the site of most morphological abnormalities I observed during analysis. This includes disorganization of the fetal vessel shape and distribution as well as maternal sinus distribution, which may be another indicator of exchange issues. Therefore, TMED2 is needed in the extraembryonic mesoderm for proper labyrinth layer formation.

To continue, through previous examinations of mutant mouse lines, embryonic lethality between E9.5-E14.5 often corresponds with large placental defects (Perez-Garcia et al., 2018). The *Tmed2*$^{loxp/loxp}$; *Mesp1*$^{Cre/+}$ mutants die by E12.5 and the reduced labyrinth layer area that we observed as well as vascular disorganization likely contribute to death. At E10, the labyrinth placenta takes over exchange from the yolk sac and we observe mutant embryos beginning to die shortly thereafter indicating the placental labyrinth may not be able to sustain the embryo (Woods et al., 2018). However, we know that *Mesp1* is expressed in other embryonic tissues, in addition to the extraembryonic region, including the heart (Saga et al., 2000). Thus, the removal of TMED2 in structures of the heart could also contribute to embryonic death, especially because heart defects are strongly associated with placental defects (Perez-Garcia et al., 2018).

Through analysis using *in situ* hybridization, I identified that *Tpbpa*, expressed by spongiotrophoblast cells above the labyrinth layer, is reduced to fewer cells in the *Tmed2*$^{loxp/loxp}$; *Mesp1*$^{Cre/+}$ mutants (El-Hashash et al., 2010). The extraembryonic mesoderm cells in the labyrinth layer that lack TMED2 may communicate to their neighbouring cells leading to this change in gene expression. I observed using the mT/mG reporter that a minority of *Mesp1*-derived cells appear near the junctional zone and spongiotrophoblast layer of the placenta. These cells and the extraembryonic mesoderm-derived cells in the labyrinth may be inhibiting normal development, expansion, and differentiation of the spongiotrophoblast cell layer. Intercellular communication is a part of developmental biology that involves various ligands and correct protein secretion or localization (Armingol et al., 2021; Basson, 2012). As TMED2 is a cargo transporter, it is plausible that a disruption in cargo transport in mutated cells can effect the neighbouring cells. This result shows that the absence of TMED2 in the extraembryonic mesoderm does not just alter the mutant cells and may be disrupting the development of other placental cells.

4.4 TMED2 is required in the extraembryonic mesoderm for normal transport and localization of some proteins

TMED2 is a transmembrane protein that acts a cargo receptor of various proteins. I found several proteins located in different cell types of the placenta labyrinth that appear to be mislocalized in the *Tmed2*$^{loxp/loxp}$; *Mesp1*$^{Cre/+}$ mutant placentas. Fibronectin, a previously identified cargo protein of TMED2, is abnormally expressed and appears to be retained in the endothelial cells in the mutants (Hou & Jerome-Majewska, 2018). Endothelial cells secrete fibronectin and are extraembryonic mesoderm-derived in the placenta (Luo & Jian, 2023; Tai-

Nagara et al., 2017). Thus, we can presume that fibronectin protein requires recognition by TMED2 in the extraembryonic mesoderm for transport. Whereas, a protein expressed on the trophoblast cells, ITGA4, also appears to require TMED2 in the extraembryonic mesoderm for correct localization (Bowen & Hunt, 1999; Johnson et al., 2023). This may be occurring since fibronectin is a binding partner of ITGA4 and since fibronectin expression is disrupted, ITGA4 becomes mislocalized (Wu et al., 1995).

TMED2 is needed in the extraembryonic mesoderm for correct MCT1 and MCT4 protein localization. These proteins are expressed in the cells of the syncytiotrophoblast bilayer, which is derived from chorion trophoblasts, not extraembryonic mesoderm (Jiang et al., 2023). In the mutant placentas, we see expression of the fusogenic genes *SynA* and *SynB* which are needed for syncytiotrophoblast layer formation (Dupressoir et al., 2011). Although the gene expression is normal, it is possible that SYNA and SYNB proteins are incorrectly localized in the syncytiotrophoblast cells preventing complete fusion of the syncytiotrophoblast layers. This could be caused by intercellular communication between the mutant cells and the syncytiotrophoblast cells. Thus, leading to a mislocalization of the proteins needed for syncytiotrophoblast layer formation or of the proteins found on these cell types. These results lead us to our working model where TMED2 is required in the extraembryonic mesoderm for normal protein localization in various cells of the labyrinth placenta (Figure 4.1).

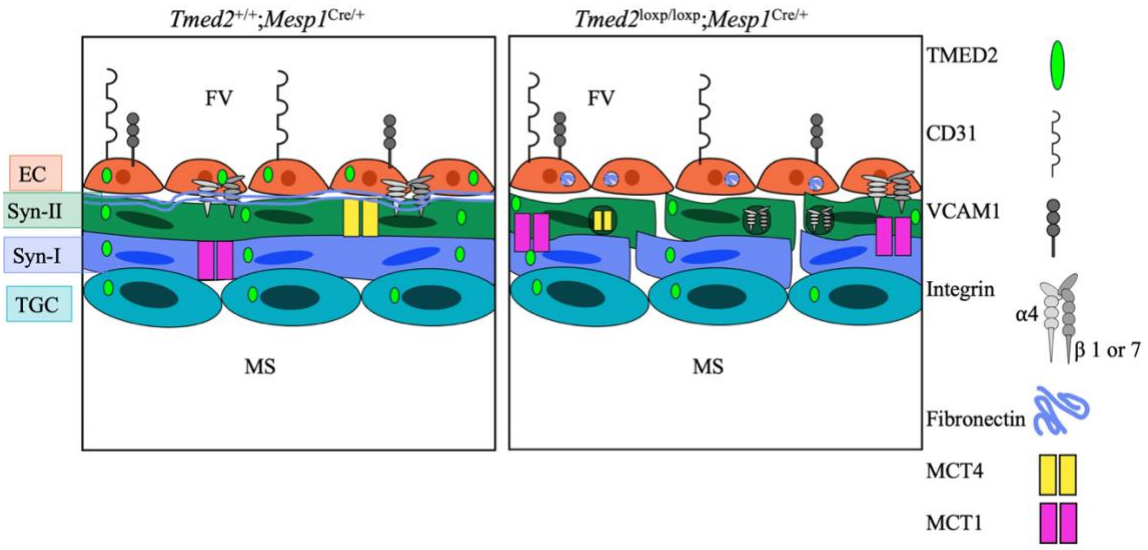

Figure 4.1. Potential model of protein transport in the cells of the *Tmed2*$^{loxp/loxp}$; *Mesp1*$^{Cre/+}$ mutant placenta labyrinth layer. Removal of TMED2 in the extraembryonic mesoderm prevents proper transport of TMED2 cargos and proteins leading to improper protein localization of those cargos and the proteins they regulate. EC: endothelial cells, Syn-II: syncytiotrophoblast-II, Syn-I: syncytiotrophoblast-I, TGC: trophoblast giant cell.

4.5 The endothelial cell proteins, CD31 and VCAM1, do not need TMED2 in the extraembryonic mesoderm for proper localization

I found that both CD31 and VCAM1 proteins were normally expressed by endothelial cells in the *Tmed2*$^{loxp/loxp}$; *Mesp1*$^{Cre/+}$ mutant placentas. These proteins are both localized to the endothelial cell surface and function as vascular adhesion molecules (Kleinhans et al., 2009). Previously, VCAM1, but not CD31, was identified as a potential TMED2 cargo protein yet it is correctly localized in these mutants (Hou & Jerome-Majewska, 2018). Transport of these

proteins may occur normally due to their recognition by other receptors in the COP-coated vesicles or through nonselective transport (Sato & Nakano, 2003). Another explanation is a possible stage-specific requirement of TMED2 for VCAM1 transport. This shows that TMED2 is not required in the extraembryonic mesoderm for the correct transport of all protein types. In the working model, we demonstrate that there is no change in the localization of these proteins on the endothelial cell surface of the fetal vessels (Figure 4.1).

CHAPTER V: CONCLUDING SUMMARY AND FUTURE DIRECTIONS

TMED2 is a transmembrane protein found in the secretory pathway where it will act as a cargo receptor to transport cargo proteins. My project focused on examining the requirement of TMED2 in the extraembryonic mesoderm. First, I characterized a new exon 2-3 deletion of *Tmed2* that produced developmentally delayed *Tmed2*$^{-/-}$ homozygous mutants. Then, I used *Mesp1*-Cre to examine placenta development when this exon 2-3 deletion of *Tmed2* occurs in the extraembryonic mesoderm. I was able to show that TMED2 is required in the extraembryonic mesoderm for normal placenta development but not labyrinth layer formation. Additionally, I found that proteins including fibronectin, ITGA4, MCT1 and MCT4 are incorrectly expressed in these mutants. I also observed normal expression of proteins expressed on the endothelial cells of the labyrinth fetal vessels, CD31 and VCAM1. Therefore, I concluded that TMED2 is needed in the extraembryonic mesoderm for transport and localization of proteins in the labyrinth layer of the placenta possibly leading to the observed morphological abnormalities.

This project focused on understanding the function of TMED2 in the placenta and specifically its requirement in the extraembryonic mesoderm. Other analyses may be done to confirm and further understand the working model. The mutant model includes disrupted protein transport in various cell types when TMED2 is absent in the extraembryonic mesoderm (Figure 4.1). We used KDEL previously to show that fibronectin was being retained in the ER. The same analysis can be done with other misexpressed proteins to determine whether they are being retained in these mutants or just mislocalized. Also, transmission electron microscopy can be used to examine the ER membranes in the cells of the placenta (Hou et al., 2017). Dilated ER membranes indicate ER stress and can lead to protein retention, this may be another explanation for the misexpressed proteins found in the *Tmed2*$^{loxp/loxp}$; *Mesp1*$^{Cre/+}$ mutant placentas (Hou &

Jerome-Majewska, 2018). Furthermore, I did not examine *Syncytin-A* expression at E11.5 as the probe did not work successfully at this stage. However, *in situ* hybridization of *Syncytin-A* could be done in the future at E11.5 to confirm continued expression of this gene and complete the analysis of the gene expression in the cells of the labyrinth layer.

Additionally, our results show the labyrinth layer forms when TMED2 is absent in the extraembryonic mesoderm. Future studies could aim to examine whether the presence of TMED2 in the extraembryonic ectoderm-derived cells is needed for labyrinth layer formation. To further examine the cell-type-specific function of TMED2, a knockout of TMED2 in the extraembryonic ectoderm would be informative. This can be done using *Cdx1-Cre,* a Cre that functions in the extraembryonic ectoderm-derived cells (Hierholzer & Kemler, 2009).

CHAPTER VI: REFERENCES

Aber, R., Chan, W., Mugisha, S., & Jerome-Majewska, L. A. (2019). Transmembrane emp24 domain proteins in development and disease. *Genetics Research*, *101*. https://doi.org/10.1017/S0016672319000090

Adamson, S. L., Lu, Y., Whiteley, K. J., Holmyard, D., Hemberger, M., Pfarrer, C., & Cross, J. C. (2002). Interactions between Trophoblast Cells and the Maternal and Fetal Circulation in the Mouse Placenta. *Developmental Biology*, *250*(2), 358-373. https://doi.org/10.1006/dbio.2002.0773

Anson-Cartwright, L., Dawson, K., Holmyard, D., Fisher, S. J., Lazzarini, R. A., & Cross, J. C. (2000). The glial cells missing-1 protein is essential for branching morphogenesis in the chorioallantoic placenta. *Nature Genetics*, *25*, 311-314. https://doi.org/10.1038/77076

Armingol, E., Officer, A., Harismendy, O., & Lewis, N. E. (2021). Deciphering cell–cell interactions and communication from gene expression. *Nature Reviews Genetics*, *22*(2), 71-88. https://doi.org/10.1038/s41576-020-00292-x

Baker, D. J. (2011). Hypomorphic mice. *Methods in Molecular Biology*, *693*, 233-244. https://doi.org/10.1007/978-1-60761-974-1_13

Barlowe, C. K., & Miller, E. A. (2013). Secretory Protein Biogenesis and Traffic in the Early Secretory Pathway. *Genetics*, *193*(2), 383-410. https://doi.org/10.1534/genetics.112.142810

Basson, M. A. (2012). Signaling in cell differentiation and morphogenesis. *Cold Spring Harbour Perspectives in Biology*, *4*(6). https://doi.org/10.1101/cshperspect.a008151

Basyuk, E., Cross, J. C., Corbin, J., Nakayama, H., Hunter, P., Nait-Oumesmar, B., & Lazzarini, R. A. (1999). Murine Gcm1 gene is expressed in a subset of placental trophoblast cells. *Developmental Dynamics*, *214*(4), 303-311. https://doi.org/10.1002/(SICI)1097-0177(199904)214:4<303::AID-AJA3>3.0.CO;2-B

Belden, W. J., & Barlowe, C. (2001). Deletion of Yeast p24 Genes Activates the Unfolded Protein Response. *Molecular biology of the cell*, *12*(4), 957-969. https://doi.org/10.1091/mbc.12.4.957

Bowen, J. A., & Hunt, J. S. (1999). Expression of Cell Adhesion Molecules in Murine Placentas and a Placental Cell Line1. *Biology of Reproduction*, *60*(2), 428-434. https://doi.org/10.1095/biolreprod60.2.428

Buechling, T., Chaudhary, V., Spirohn, K., Weiss, M., & Boutros, M. (2011). p24 proteins are required for secretion of Wnt ligands. *EMBO reports*, *12*(12), 1265-1272. https://doi.org/0.1038/embor.2011.212.

Burton, G. J., & Fowden, A. L. (2015). The placenta: a multifaceted, transient organ. *Philosophical transactions of the Royal Society of London. Series B, Biological sciences*, *370*(1663), 20140066. https://doi.org/10.1098/rstb.2014.0066

Carney, G. E., & Bowen, N. J. (2004). p24 proteins, intracellular trafficking, and behavior: Drosophila melanogaster provides insights and opportunities. *Biology of the cell*, *96*(4), 271–278. https://doi.org/10.1016/j.biolcel.2004.01.004

Cela, I., Dufrusine, B., Rossi, C., Luini, A., Laurenzi, V. D., Federici, L., & Sallese, M. (2022). KDEL Receptors: Pathophysiological Functions, Therapeutic Options, and Biotechnological Opportunities. *Biomedicines*, *10*(6), 1234. https://doi.org/10.3390/biomedicines10061234

Charalambous, C., Drakou, K., Nicolaou, S., & Georgiades, P. (2013). Novel spatiotemporal glycome changes in the murine placenta during placentation based on BS-I lectin binding patterns. *The Anatomical Record*, *296*(6), 921-932. https://doi.org/10.1002/ar.22698

Christodoulou, N., Weberling, A., Strathdee, D., Anderson, K. I., Timpson, P., & Zernicka-Goetz, M. (2019). Morphogenesis of extra-embryonic tissues directs the remodelling of the mouse embryo at implantation. *Nature Communications*, *10*(1), 3557. https://doi.org/10.1038/s41467-019-11482-5

Cole, N. B., Ellenberg, J., Song, J., DiEuliis, D., & Lippincott-Schwartz, J. (1998). Retrograde Transport of Golgi-localized Proteins to the ER. *Journal of Cell Biology*, *140*(1), 1-15. https://doi.org/10.1083/jcb.140.1.1

Cross, J. C., Nakano, H., Natale, D. R. C., Simmons, D. G., & Watson, E. D. (2006). Branching morphogenesis during development of placental villi. *Differentiation*, *74*(7), 393-401. https://doi.org/https://doi.org/10.1111/j.1432-0436.2006.00103.x

Cross, J. C., Simmons, D. G., & Watson, E. D. (2003). Chorioallantoic Morphogenesis and Formation of the Placental Villous Tree. *Annals of the New York Academy of Sciences*, *995*, 84-93. https://doi.org/10.1111/j.1749-6632.2003.tb03212.x

Dominguez, M., Dejgaard, K., Füllekrug, J., Dahan, S., Fazel, A., Paccaud, J., Thomas, D., Bergeron, J., & Nilsson, T. (1998). gp25L/emp24/p24 protein family members of the cis-Golgi network bind both COP I and II coatomer. *The Journal of cell biology*, *140*(4), 751–765. https://doi.org/10.1083/jcb.140.4.751

Donaldson, J. G., & Lippincott-Schwartz, J. (2000). Sorting and Signaling at the Golgi Complex. *Cell*, *101*(7), 693-696. https://doi.org/10.1016/S0092-8674(00)80881-8

Downs, K. M. (2022). The mouse allantois: new insights at the embryonic–extraembryonic interface. *Philosophical Transactions of the Royal Society B: Biological Sciences*, *377*(1865). https://doi.org/10.1098/rstb.2021.0251

Duden, R. (2003). ER-to-Golgi transport: COP I and COP II function (Review). *Molecular membrane biology*, *20*(3), 197-207. https://doi.org/10.1080/0968768031000122548

Dupressoir, A., Vernochet, C., Harper, F., Guégan, J., Dessen, P., Pierron, G., & Heidmanna, T. (2011). A pair of co-opted retroviral envelope syncytin genes is required for formation of the two-layered murine placental syncytiotrophoblast. *Proceedings of the National Academy of Sciences of the United States of America*, *108*(46), E1164–E1173. https://doi.org/10.1073/pnas.1112304108

El-Hashash, A. H. K., Warburton, D., & Kimber, S. J. (2010). Genes and signals regulating murine trophoblast cell development. *Mechanisms of Development*, *127*(1), 1-20. https://doi.org/10.1016/j.mod.2009.09.004

Elmore, S. A., Cochran, R. Z., Bolon, B., Lubeck, B., Mahler, B., Sabio, D., & Jerrold M Ward. (2022). Histology Atlas of the Developing Mouse Placenta. *Toxicologic Pathology*, *50*(1), 60-117. https://doi.org/10.1177/01926233211042270

Faria, T. N., Ogren, L., Talamantes, F., Linzer, D. I. H., & Soares, M. J. (1991). Localization of Placental Lactogen-l in Trophoblast Giant Cells of the Mouse Placenta. *Biology of Reproduction*, *44*(2), 327-331. https://doi.org/10.1095/biolreprod44.2.327

Gardner, R., Papaioannou, V., & Barton, S. (1973). Origin of the ectoplacental cone and secondary giant cells in mouse blastocysts reconstituted from isolated trophoblast and inner cell mass. *Development*, *30*(3), 561-572. https://doi.org/10.1242/dev.30.3.561

Gurtner, G. C., Davis, V., Li, H., McCoy, M. J., Sharpe, A., & Cybulsky, M. I. (1995). Targeted disruption of the murine VCAM1 gene: essential role of VCAM-1 in chorioallantoic fusion and placentation. *Genes & Development*, *9*(1). https://doi.org/10.1101/gad.9.1.1

Hierholzer, A., & Kemler, R. (2009). Cdx1::Cre allele for gene analysis in the extraembryonic ectoderm and the three germ layers of mice at mid-gastrulation. *Genesis*, *47*(3), 204-209. https://doi.org/10.1002/dvg.20484

Hou, W., Gupta, S., Beauchamp, M. C., Yuan, L., & Jerome-Majewska, L. A. (2017). Non-alcoholic fatty liver disease in mice with heterozygous mutation in TMED2. *PLoS One*, *12*(8), e0182995. https://doi.org/10.1371/journal.pone.0182995

Hou, W., & Jerome-Majewska, L. A. (2018). TMED2/emp24 is required in both the chorion and the allantois for placental labyrinth layer development. *Developmental Biology*, *444*(1), 20-32. https://doi.org/10.1016/j.ydbio.2018.09.012

Hou, W., Sarikaya, D. P., & Jerome-Majewska, L. A. (2016). Ex vivo culture of pre-placental tissues reveals that the allantois is required for maintained expression of Gcm1 and Tpbpa. *Placenta*, *47*, 12-23. https://doi.org/10.1016/j.placenta.2016.08.091

Hsiao, C.-T., Cheng, H.-W., Huang, C.-M., Li, H.-R., Ou, M.-H., Huang, J.-R., Khoo, K.-H., Yu, H. W., Chen, Y.-Q., Wang, Y.-K., Chiou, A., & Kuo, J.-C. (2017). Fibronectin in cell adhesion and migration via N-glycosylation. *Oncotarget*, *8*(41), 70653-70668. https://doi.org/10.18632/oncotarget.19969

Hu, D., & Cross, J. C. (2011). Ablation of Tpbpa-positive trophoblast precursors leads to defects in maternal spiral artery remodeling in the mouse placenta. *Developmental Biology*, *358*(1), 231-239.

Inman, K., & Downs, K. (2007). The murine allantois: emerging paradigms in development of the mammalian umbilical cord and its relation to the fetus. *Genesis*, *45*(5), 237-258. https://doi.org/10.1002/dvg.20281

Jerome-Majewska, L. A., Achkar, T., Luo, L., Lupu, F., & Lacy, E. (2010). The trafficking protein Tmed2/p24beta(1) is required for morphogenesis of the mouse embryo and placenta. *Developmental Biology*, *341*(1), 154-166. https://doi.org/10.1016/j.ydbio.2010.02.019

Jiang, X., Wang, Y., Xiao, Z., Yan, L., Guo, S., Wang, Y., Wu, H., Zhao, X., Lu, X., & Wang, H. (2023). A differentiation roadmap of murine placentation at single-cell resolution. *Cell Discovery*, *9*. https://doi.org/10.1038/s41421-022-00513-z

John, R., & Hemberger, M. (2012). A placenta for life. *Reproductive BioMedicine*, *25*, 5-11. https://doi.org/10.1016/j.rbmo.2012.03.018

Johnson, G. A., Burghardt, R. C., Bazer, F. W., Seo, H., & Cain, J. W. (2023). Integrins and their potential roles in mammalian pregnancy. *Journal of Animal Science and Biotechnology*, *14*(1), 115. https://doi.org/10.1186/s40104-023-00918-0

Kim, H., Kim, M., Im, S. K., & Fang, S. (2018). Mouse Cre-LoxP system: general principles to determine tissue-specific roles of target genes. *Lab Anim Res*, *34*(4), 147-159. https://doi.org/10.5625/lar.2018.34.4.147

Kleinhans, H., Kaifi, J. T., Mann, O., Reinknecht, F., Freitag, M., Hansen, B., Schurr, P. G., Izbicki, J. R., & Strate, T. G. (2009). The role of vascular adhesion molecules PECAM-1 (CD 31), VCAM-1 (CD 106), E-selectin (CD62E) and P-selectin (CD62P) in severe porcine pancreatitis. *Histol Histopathol*, *24*(5), 551-557. https://doi.org/10.14670/hh-24.551

Kong, D.-H., Kim, Y. K., Kim, M. R., Jang, J. H., & Lee, S. (2018). Emerging Roles of Vascular Cell Adhesion Molecule-1 (VCAM-1) in Immunological Disorders and Cancer. *International Journal of Molecular Sciences*, *19*(4), 1057. https://doi.org/10.3390/ijms19041057

Kwee, L., Baldwin, H., Shen, H., Stewart, C., Buck, C., Buck, C., & Labow, M. (1995). Defective development of the embryonic and extraembryonic circulatory systems in vascular cell adhesion molecule (VCAM-1) deficient mice. *Development*, *121*(2), 489-503. https://doi.org/10.1242/dev.121.2.489

Lawless, L., Qin, Y., Xie, L., & Zhang, K. (2023). Trophoblast Differentiation: Mechanisms and Implications for Pregnancy Complications. *Nutrients*, *15*(16). https://doi.org/10.3390/nu15163564

Lertkiatmongkol, P., Liao, D., Mei, H., Hu, Y., & Newmana, P. J. (2016). Endothelial functions of PECAM-1 (CD31). *Current Opinion in Hematology*, *23*(3), 253-259. https://doi.org/10.1097/MOH.0000000000000239

Liu, Y., Chen, L., Diaz, A. D., Benham, A., Xu, X., Wijaya, C. S., Fa'ak, F., Luo, W., Soibam, B., Azares, A., Yu, W., Lyu, Q., Stewart, M. D., Gunaratne, P., Cooney, A., McConnell, B. K., & Schwartz, R. J. (2016). Mesp1 Marked Cardiac Progenitor Cells Repair Infarcted Mouse Hearts. *Scientific Reports*, *6*(1), 31457. https://doi.org/10.1038/srep31457

Luo, W., Wang, Y., & Reiser, G. (2007). p24A, a Type I Transmembrane Protein, Controls ARF1-dependent Resensitization of Protease-activated Receptor-2 by Influence on Receptor Trafficking. *The Journal of biological chemistry*, *282*(41), 30246-30255. https://doi.org/10.1074/jbc.M703205200

Luo, X., & Jian, W. (2023). Different roles of endothelial cell-derived fibronectin and plasma fibronectin in endothelial dysfunction. *Turkish Journal of Medical Sciences*, *53*(6), 1667-1677. https://doi.org/10.55730/1300-0144.5735

Luzio, J. P., Hackmann, Y., Dieckmann, N. M. G., & Griffiths, G. M. (2014). The Biogenesis of Lysosomes and Lysosome-Related Organelles. *Cold Spring Harbor Perspectives in Biology*, *6*(9), a016840. https://doi.org/10.1101/cshperspect.a016840

Marzioch, M., Henthorn, D., Herrmann, J., Wilson, R., Thomas, D., Bergeron, J., Solari, R., & Rowley, A. (1999). Erp1p and Erp2p, partners for Emp24p and Erv25p in a yeast p24 complex. *Molecular biology of the cell 10*(6), 1923–1938. https://doi.org/10.1091/mbc.10.6.1923

Matsuo, I., & Hiramatsu, R. (2017). Mechanical perspectives on the anterior-posterior axis polarization of mouse implanted embryos. *Mechanisms of Development*, *144*, 62-70. https://doi.org/10.1016/j.mod.2016.09.002

Minin, G. D., Holzner, M., Grison, A., Dumeau, C. E., Chan, W., Monfort, A., Jerome-Majewska, L. A., Roelink, H., & Wutz, A. (2022). TMED2 binding restricts SMO to the ER and Golgi compartments. *PLoS Biol*, *20*(3), e3001596. https://doi.org/10.1371/journal.pbio.3001596

Morris, S. A. (2011). Cell fate in the early mouse embryo: sorting out the influence of developmental history on lineage choice. *Reproductive BioMedicine Online*, *22*, 521–524. https://doi.org/10.1016/j.rbmo.2011.02.009

Muniz, M., Nuoffer, C., Hauri, H. P., & Riezman, H. (2000). The Emp24 complex recruits a specific cargo molecule into endoplasmic reticulum-derived vesicles. *Journal of Cell Biology*, *148*(5), 925–930. https://doi.org/10.1083/jcb.148.5.925

Muzumdar, M. D., Tasic, B., Miyamichi, K., Li, L., & Luo, L. (2007). A global double-fluorescent Cre reporter mouse. *Genesis*, *45*, 593-605. https://doi.org/10.1002/dvg.20335

Nadeau, V., & Charron, J. (2014). Essential role of the ERK/MAPK pathway in blood-placental barrier formation. *Development*, *141*(14), 2825-2837. https://doi.org/10.1242/dev.107409

Nagae, M., Hirata, T., Morita-Matsumoto, K., Theiler, R., Fujita, M., Kinoshita, T., & Yamaguchi, Y. (2016). 3D Structure and Interaction of p24β and p24δ Golgi Dynamics Domains: Implication for p24 Complex Formation and Cargo Transport. *Journal of Molecular Biology*, *428*(20), 4087-4099. https://doi.org/10.1016/j.jmb.2016.08.023.

Nagai, A., Takebe, K., Nio-Kobayashi, J., Takahashi-Iwanaga, H., & Iwanaga, T. (2010). Cellular Expression of the Monocarboxylate Transporter (MCT) Family in the Placenta of Mice. *Placenta*, *31*(2), 126-133. https://doi.org/10.1016/j.placenta.2009.11.013

Okamura, K., Kimata, Y., Higashio, H., Tsuru, A., & Kohno, K. (2000). Dissociation of Kar2p/BiP from an ER Sensory Molecule, Ire1p, Triggers the Unfolded Protein Response in Yeast. *Biochemical and Biophysical Research Communications*, *279*(2), 445-450. https://doi.org/10.1006/bbrc.2000.3987.

Panja, S., & Paria, B. (2021). Development of the Mouse Placenta. *Advances in Anatomy, Embryology and Cell Biology*, *234*, 205-221. https://doi.org/10.1007/978-3-030-77360-1_10

Pelham, H. R. (1996). The dynamic organisation of the secretory pathway. *Cell structure and function*, *21*(5), 413-419. https://doi.org/10.1247/csf.21.413

Perez-Garcia, V., Fineberg, E., Wilson, R., Murray, A., Mazzeo, C. I., Tudor, C., Sienerth, A., White, J. K., Tuck, E., Ryder, E. J., Gleeson, D., Siragher, E., Wardle-Jones, H., Staudt, N., Wali, N., Collins, J., Geyer, S., Busch-Nentwich, E. M., Galli, A., . . . Hemberger, M.

(2018). Placentation defects are highly prevalent in embryonic lethal mouse mutants. *Nature*, *555*(7697), 463-468. https://doi.org/10.1038/nature26002

Rinkenberger, J., & Werb, Z. (2000). The labyrinthine placenta. *Nature Genetics*, *25*(3), 248-250. https://doi.org/10.1038/76985

Roberts, B. S., & Satpute-Krishnan. (2023). The many hats of transmembrane emp24 domain protein TMED9 in secretory pathway homeostasis. *Frontiers in Cell and Developmental Biology*, *10*. https://doi.org/10.3389/fcell.2022.1096899

Rusidzé, M., Gargaros, A., Fébrissy, C., Dubucs, C., Weyl, A., Ousselin, J., Aziza, J., Arnal, J.-F., & Lenfant, F. (2023). Estrogen Actions in Placental Vascular Morphogenesis and Spiral Artery Remodeling: A Comparative View between Humans and Mice. *Cells*, *12*(4), 620. https://www.mdpi.com/2073-4409/12/4/620

Saga, Y., Hata, N., Kobayashi, S., Magnuson, T., Seldin, M. F., & Taketo, M. M. (1996). MesP1: a novel basic helix-loop-helix protein expressed in the nascent mesodermal cells during mouse gastrulation. *Development*, *122*(9), 2769–2778. https://doi.org/10.1242/dev.122.9.2769

Saga, Y., Kitajima, S., & Miyagawa-Tomita, S. (2000). Mesp1 Expression Is the Earliest Sign of Cardiovascular Development. *Trends in Cardiovascular Medicine*, *10*(8), 345-352. https://doi.org/10.1016/S1050-1738(01)00069-X

Saga, Y., Miyagawa-Tomita, S., Takagi, A., Kitajima, S., Miyazaki, J.-i., & Inoue, T. (1999). MesP1 is expressed in the heart precursor cells and required for the formation of a single heart tube. *Development*, *126*(15), 3437-3447. https://doi.org/10.1242/dev.126.15.3437

Sato, K., & Nakano, A. (2003). Oligomerization of a cargo receptor directs protein sorting into COPII-coated transport vesicles. *Molecular biology of the cell*, *14*(7), 3055-3063. https://doi.org/10.1091/mbc.e03-02-0115

Saylam, C., Özdemir, N., Itil, I. M., Sendag, F., & Terek, M. C. (2002). Distribution of fibronectin, laminin and collagen type IV in the materno-fetal boundary zone of the developing mouse placenta. *Archives of Gynecology and Obstetrics*, *266*(2), 83-85. https://doi.org/10.1007/s004040100204

Schwarz, D. S., & Blower, M. D. (2016). The endoplasmic reticulum: structure, function and response to cellular signaling. *Cellular and Molecular Life Sciences*, *23*(1), 79-94. https://doi.org/10.1007/s00018-015-2052-6

Shaha, S., Patel, K., & Riddell, M. (2023). Cell polarity signaling in the regulation of syncytiotrophoblast homeostasis and inflammatory response. *Placenta*, *141*, 26-34. https://doi.org/10.1016/j.placenta.2022.11.007

Simmons, D., Fortier, A., & Cross, J. (2007). Diverse subtypes and developmental origins of trophoblast giant cells in the mouse placenta. *Developmental Biology*, *304*(2), 567-578. https://doi.org/10.1016/j.ydbio.2007.01.009

Simmons, D. G., & Cross, J. C. (2005). Determinants of trophoblast lineage and cell subtype specification in the mouse placenta. *Developmental Biology*, *284*(1), 12-24. https://doi.org/10.1016/j.ydbio.2005.05.010.

Simmons, D. G., Natale, D. R. C., Begay, V., Hughes, M., Leutz, A., & Cross, J. C. (2008). Early patterning of the chorion leads to the trilaminar trophoblast cell structure in the placental labyrinth. *Development*, *135*(12), 2083-2091. https://doi.org/10.1242/dev.020099

Singh, P., Carraher, C., & Schwarzbauer, J. E. (2010). Assembly of Fibronectin Extracellular Matrix. *Annual Review of Cell and Developmental Biology*, *26*, 397-419. https://doi.org/10.1146/annurev-cellbio-100109-104020

Soares, M. J., Varberg, K. M., & Iqbal, K. (2018). Hemochorial placentation: development, function, and adaptations. *Biology of Reproduction*, *99*(1), 196-211. https://doi.org/10.1093/biolre/ioy049

Spang, A. (2013). Retrograde Traffic from the Golgi to the Endoplasmic Reticulum. *Cold Spring Harbor Perspectives in Biology*, *5*(6), a013391. https://doi.org/10.1101/cshperspect.a013391

Stecca, B., Nait-Oumesmar, B., Kelley, K. A., Voss, A. K., Thomas, T., & Lazzarini, R. A. (2002). Gcm1 expression defines three stages of chorio-allantoic interaction during placental development. *Mechanisms of Development*, *115*(1), 27-34. https://doi.org/https://doi.org/10.1016/S0925-4773(02)00095-3

Stirling, C., Rothblatt, J., Hosobuchi, M., Deshaies, R., & Schekman, R. (1992). Protein translocation mutants defective in the insertion of integral membrane proteins into the endoplasmic reticulum. *Molecular biology of the cell 3*(2), 129-142. https://doi.org/10.1091/mbc.3.2.129

Strating, J. R. P. M., & Martens, G. J. M. (2009). The p24 family and selective transport processes at the ER—Golgi interface. *Biology of the cell*, *101*(9), 495-509. https://doi.org/10.1042/BC20080233

Tai-Nagara, I., Yoshikawa, Y., Numata, N., Ando, T., Okabe, K., Sugiura, Y., Ieda, M., Takakura, N., Nakagawa, O., Zhou, B., Okabayashi, K., Suematsu, M., Kitagawa, Y., Bastmeyer, M., Sato, K., Klein, R., Navankasattusas, S., Li, D. Y., Yamagishi, S., & Kubota, Y.

(2017). Placental labyrinth formation in mice requires endothelial FLRT2/UNC5B signaling. *Development 144*(13), 2392-2401. https://doi.org/10.1242/dev.149757

Watson, E. D., & Cross, J. C. (2005). Development of structures and transport functions in the mouse placenta. *Physiology*, *20*(3), 180-193. https://doi.org/10.1152/physiol.00001.2005

Wen, C., & Greenwald, I. (1999). p24 proteins and quality control of LIN-12 and GLP-1 trafficking in Caenorhabditis elegans. *J Cell Biol*, *145*(6), 1165-1175. https://doi.org/10.1083/jcb.145.6.1165

Woods, L., Perez-Garcia, V., & Hemberger, M. (2018). Regulation of Placental Development and Its Impact on Fetal Growth-New Insights From Mouse Models. *Frontiers in Endocrinology*, *9*, 570. https://doi.org/10.3389/fendo.2018.00570

Wu, C. (1997). Roles of integrins in fibronectin matrix assembly. *Histology and Histopathology*, *12*, 233-240. https://doi.org/10.14670/HH-12.233

Wu, C., Fields, A. J., Kapteijn, B. A. E., & McDonald, J. A. (1995). The role of α4β1 integrin in cell motility and fibronectin matrix assembly. *Journal of Cell Science*, *108*(2), 821-829. https://doi.org/10.1242/jcs.108.2.821

Yang, F., Huang, L., Tso, A., Wang, H., Cui, L., Lin, L., Wang, X., Ren, M., Fang, X., Liu, J., Han, Z., Chen, J., & Ouyang, K. (2020). Inositol 1,4,5-trisphosphate receptors are essential for fetal-maternal connection and embryo viability. *PLoS genetics*, *16*(4). https://doi.org/10.1371/journal.pgen.1008739

Yung, H. W., Hemberger, M., Watson, E. D., Senner, C. E., Jones, C. P., Kaufman, R. J., Charnock-Jones, D. S., & Burton, G. J. (2012). Endoplasmic reticulum stress disrupts placental morphogenesis: implications for human intrauterine growth restriction. *J Pathol*, *228*(4), 554-564. https://doi.org/10.1002/path.4068

Zakariyah, A., Hou, W., Slim, R., & Jerome-Majewska, L. (2012). TMED2/p24beta1 is expressed in all gestational stages of human placentas and in choriocarcinoma cell lines. *Placenta*, *33*(3), 214-219. https://doi.org/10.1016/j.placenta.2011.12.009

Zhou, L., Li, H., Yao, H., Dai, X., Gao, P., & Cheng, H. (2023). TMED family genes and their roles in human diseases. *International Journal of Medical Sciences*, *20*(13), 1732–1743. https://doi.org/10.7150/ijms.87272

Zhu, D., Gong, X., Miao, L., Fang, J., & Zhang, J. (2017). Efficient Induction of Syncytiotrophoblast Layer II Cells from Trophoblast Stem Cells by Canonical Wnt Signaling Activation. *Stem Cell Reports*, *9*(6), 2034-2049. https://doi.org/10.1016/j.stemcr.2017.10.014

COPYRIGHT

Figure 1.2:

Figure 1.3: